TECHNISCHE UNIVERSITÄT WIEN

Diplomarbeit

Characterization and classification of Epoxy Molding compounds using LIBS and LA-ICP-MS

carried out at

Institute of Chemical Technologies and Analytics

TU Wien

under the supervision of

Univ.Prof. Dipl.-Ing. Dr.techn. Andreas Limbeck

Dipl.-Ing. Dr.techn. Lukas Brunnbauer, BSc

by

Veronika Zeller

date

signature

Abstract

Electronic devices are ever-present in our day-to-day lives. Integrated circuits are built into our vehicles (trains, planes, ships, cars) and into medical equipment, where the failure of the device can have potentially catastrophic consequences. For this reason, the reliability of their products is of great concern to chip manufacturers. The silicon die at the heart of an integrated circuit and the bond wires connecting it to its pins is encapsulated in a packaging material, most commonly an epoxy based polymer with complex inorganic additives and fillers, called molding compound. Its purpose is to protect against outside influences such as corrosive atmospheres (moisture) or mechanical stress. Chip Manufacturers obtain this material from a specialized polymer manufacturer, and have limited insight into its exact composition. As it is in direct contact with the silicon die and delicate wiring, its physical and chemical properties can directly affect the chip's performance. This makes the choice of an appropriate material crucial for a device's reliability. A tool to identify different molding compounds correctly and to detect changes in the composition caused by contamination would therefore be very useful for the chip manufacturers' quality assurance.

In this work, the goal was to characterize 29 samples of 20 molding compounds from four suppliers, as well as to develop a classification model that could potentially be applied to identify unknown sample types correctly. Initial insights about the composition of different samples were collected using inductively coupled plasma mass spectrometry (ICP-MS) after microwave assisted acid digestion. Laser induced breakdown spectroscopy (LIBS) and Tandem LIBS-laser ablation ICP-MS measurements were performed on all available samples to collect a comprehensive set of data with the goal of identifying elemental patterns that contain information about the utilized materials and potential contaminations. Multivariate data analysis methods such as principal component analysis and distance-based clustering were used for exploratory data analysis. Classification models based on random decision forest classifiers were trained and the performance of the classifiers based on the LIBS set and the Tandem LIBS/LA-ICP-MS set were compared using measurement data of held back test samples.

LIBS and LA-ICP-MS measurements proved to be well suited for the investigation of molding compound samples. Exploratory data analysis on a LIBS and a tandem LIBS/LA-ICP-MS dataset revealed patterns in the content of some major inorganic components, like Si and Zn, dependent on the manufacturer and in the content of minor inorganic components such as Zr, Mn, Ce, Pr and Nd dependent on the molding compound. In total, more than 20 elements could be detected in the solid samples using LIBS and LA-ICP-MS. In some cases, samples of different molding compounds turned out to be more similar to each other than to samples of the same type. Careful selection of spectral descriptors allowed the generation of random decision forest models that achieved a Matthew's correlation coefficient in cross validation above 95 % for all molding compound types and both datasets. These models could correctly classify the majority of held back test samples, but confused some of the very similar ones. The classifier built solely on LIBS data performed slightly better than the classifier built on tandem data, with a possible explanation being the better quality of the LIBS data and the exclusion of potentially misleading trace elements. To improve on the performance of the classification, a bigger dataset containing multiple samples of each dataset could be measured to build a more stable classifier.

Kurzfassung

Wir sind in unserem Alltag von Elektronik umgeben. Integrierte Schaltkreise finden sich in vielen kritischen Anwendungsbereichen, wie dem Verkehr (in Zügen, Flugzeugen, Schiffen und Autos) oder dem medizinischen Bereich, mit potenziell dramatischen Konsequenzen bei Ausfällen und Fehlfunktionen. Für Chiphersteller ist aus diesem Grund die Zuverlässigkeit ihrer Produkte von großer Bedeutung. Der eigentliche Siliziumchip und die Drahtverbindungen die ihn mit seinen Kontakten verbinden sind von einem Material umhüllt, das sie vor äußeren Einflüssen schützt. Beispiele für potentiell schädliche äußere Einflüsse sind atmosphärische Einflüsse wie Feuchtigkeit oder mechanische Belastung. Meist handelt es sich um komplexe Kunststoffe auf Epoxidbasis mit einem hohen Anteil an anorganischen Füllstoffen und Additiven, die als „Epoxy Molding compounds“ bezeichnet werden. Chiphersteller kaufen sie bei spezialisierten Fabrikanten zu und haben nur begrenzt Einblick in die exakte Zusammensetzung des Materials. Aufgrund des direkten Kontakts zwischen Molding Compound und dem Siliziumchip sowie den empfindlichen Bonddrähten haben die chemischen und physikalischen Eigenschaften des Hüllmaterials direkten Einfluss auf die Zuverlässigkeit des Bauteils. Eine Möglichkeit, verschiedene Molding Compounds verlässlich zu identifizieren und Unterschiede in der Zusammensetzung bzw. Veränderungen, die eventuell durch Verunreinigungen verursacht wurden, zu erkennen wäre deshalb äußerst nützlich für die Qualitätssicherung der Chiphersteller.

Ziel dieser Arbeit war die Charakterisierung von 29 Molding Compound Proben (20 verschieden Typen) vierer Fabrikanten sowie die Entwicklung eines Modells zur korrekten Klassifizierung unbekannter Proben. Erste Einblicke in die Elementarzusammensetzung einiger Proben lieferten ICP-MS Messungen nach mikrowellenunterstütztem Säureaufschluss. Von allen Proben wurden LIBS und Tandem LIBS/LA-ICP-MS Messungen durchgeführt, um einen umfangreichen Datensatz zu sammeln, anhand dessen Muster in der elementaren Zusammensetzung sichtbar gemacht werden sollten, die Information über die verwendeten Materialien und eventuelle Verunreinigungen enthalten. Dieser wurde anhand einer Hauptkomponentenanalyse sowie einer Clusteranalyse untersucht. Klassifikatoren basierend auf einen Random Forest Algorithmus wurden trainiert und anhand eines zurückgehaltenen Testsets verglichen.

LIBS und LA-ICP-MS stellte sich als sehr geeignet für die Messung von Molding Compound heraus. Die Untersuchung eines LIBS und eines Tandem LIBS/LA-ICP-MS Datensatzes enthüllte Muster im Gehalt einiger anorganischer Hauptbestandteile, wie Si und Zn in Abhängigkeit vom Hersteller. Der Gehalt an anorganischen Nebenbestandteilen wie Zr, Mn, Ce, Pr und Nd zeigte eine Abhängigkeit vom Molding Compound Typ. In einzelnen Fällen war der Unterschied zwischen Proben vom selben Molding Compound größer als zwischen Proben verschiedener Molding Compounds. Sorgfältige Auswahl der spektralen Deskriptoren ermöglichte die Erzeugung von Random Forest Modellen aus beiden Datensätzen, die in der Kreuzvalidierung einen Matthews Korrelationskoeffizienten größer 95 % für alle Molding Compound Typen erzielten. Diese Modelle waren in der Lage, bei der Modellerstellung zurückgehaltene Proben in der Mehrheit der Fälle richtig zuzuordnen, verwechselten jedoch einzelne sehr ähnliche Molding Compounds. Der nur auf LIBS-Daten basierende Klassifikator erzielte etwas bessere Ergebnisse als jener der aus Tandem Daten erstellt wurde, was eventuell durch die höhere Qualität der LIBS Daten und die Abwesenheit potentiell irreführender Informationen über Spurenbestandteile zu erklären ist. Um die Klassifizierung zu verbessern wäre es möglich einen umfassenderen Datensatz mit mehreren Proben von jedem Molding Compound zu generieren um einen stabileren Klassifikator zu erstellen.

Acknowledgements

At this place, I would like to express my gratitude and thanks to all the wonderful people that supported me in completing this thesis.

I would like to thank Andreas Limbeck, for giving me the opportunity to work on such an interesting topic and for always taking the time and showing interest when I came to him with any concerns. I am deeply grateful to Lukas Brunnbauer, whose enthusiasm for analytical chemistry was as invaluable to me as his guidance and advice on practical aspects of my work and his support during the writing process. Hans Lohninger, who put his wealth of knowledge regarding chemometry and its application at my disposal during long hours of discussion, I would like to thank for handing me the tools for data analysis, both figuratively and literally.

I would like to acknowledge Infineon technologies, for their help in procuring the samples and their efforts supporting this work financially and providing information and expert knowledge. Special thanks goes to Stefan Schwab for patiently answering questions and for providing a positive working environment across continents.

The other master students and members of the research group, I would like to thank for taking an interest, listening and providing feedback on drafts and presentations and for help with instrument problems. Whenever I needed help, someone was there.

Finally, this acknowledgement would not be complete without a thank you to my family, for all the emotional as well as the financial support. Without you, none of this would have been possible.

Contents

1 Introduction

In our day to day lives, microelectronics are ever-present. The value of the global semiconductor market was 450 billion US dollars in 2021 and is projected to grow to nearly 900 billion dollars by 2029 [1]. Reason for this growth is increasing demand for consumer electronics, as well as increasing demand for integrated circuits [1]. Integrated circuits combine a high amount of functionality on small semiconductor chips[2], which saves space and facilitates smaller devices. We use electronic devices for work and entertainment but integrated circuits are also built into our cars, trains, ships and planes, into medical equipment[3], into early warning systems for earthquakes[4] and into fire warning devices[5], and many other appliances where reliability is essential.

Modern integrated circuits can take many forms, depending on their application, but the general structure is similar for most of them. Figure 1 depicts a schematic view of a dual in-line package, a common type of integrated circuit package. At the heart of the device is a semiconductor die, made from Si, SiGe, GaN, SiC, InP or GaAs, with the electronic circuits responsible for the devices functionality[6], [7]. The semiconductor die is attached to a substrate, such as a leadframe pad, and the electronic circuits' inputs and outputs are connected to the leadframe by thin gold, copper or aluminium wires[8], [9]. The whole construct is then enclosed in a packaging material, with only the leads sticking out. The packaging most often is made from a specialised type of polymer[6], the most widely used being epoxy molding compounds[10]. In addition to the base polymer, molding compounds generally contain a multitude of inorganic fillers and (in)organic additives, such as hardeners, accelerators and flame-retardants[10]

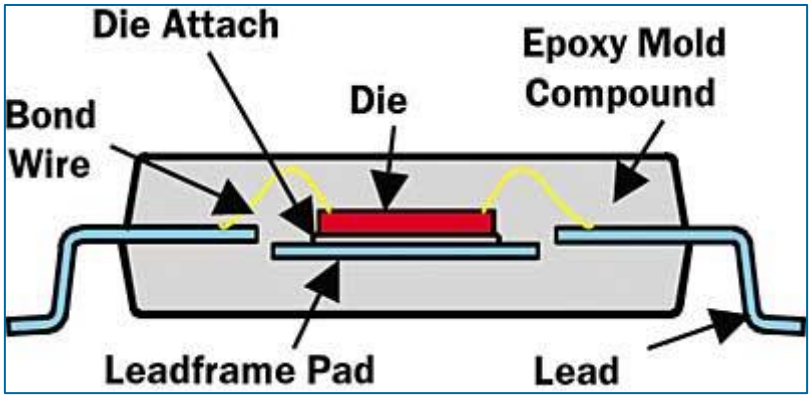

Figure 1: Example for an integrated circuit package, from[11].

The packaging of the integrated circuit primarily fulfills the purpose of providing protection of the semiconductor die and delicate bond wires against external influences such as moisture and mechanical stress. Since the packaging material is in direct contact with the semiconductor die and bond wires, its properties directly influence the reliability and must be chosen carefully to avoid device failure due to warpage[12], layering and cracking[13] or corrosion caused by moisture intrusion[13].

Research into contributing factors to failure of electronic devices by the molding compound encapsulation material is ongoing. For electronic components used in high temperature environments, such as car engines, high temperature aging of the polymer has been studied. Oxidation of the polymer material causes changes to the mechanical properties, such as the density, resulting in cracking of the oxidised layer[14]–[16]. A high content of silica powder as filling material was observed to inhibit the oxidisation process[17]. Moisture absorbed by the polymer causes multiple problems, such as corrosion of the Al bonding pad and delamination[18]–[20]. A high adhesion strength and low Young's modulus are reported to reduce the delamination risk[20]. In addition to oxygen and moisture, the diffusion and migration of different ionic species through the encapsulation material has been observed to influence the reliability of the electronic device by means of corrosion of metal components or dendritic growth[21], as well as chip failure due to a shift in threshold voltage of the transistor[22]. A study using diffusion cells and secondary ion mass spectrometry to investigate Sodium and Chloride ion diffusion in molding compounds

has been published[23], stating a connection between the ion diffusion rate and the molding compound formulation. Diffusion of silver ions was investigated, showing a dependence of migration rate on molding compound formulation[24].

The chip manufacturer encapsulates the integrated circuit in the packaging material, but specialized polymer manufacturers supply the material. Typically, a wide range of different mold compound types with fine-tuned compositions for various semiconductor products are available. Since the exact composition is only known by the supplier, chip manufacturers are in need of comprehensive tools for quality assurance. These tools have to be capable of characterizing and classifying the obtained materials to make sure the correct material was delivered, and its properties do not deviate from previous batches.

Commonly employed tools for such an analysis would be FT-IR and Raman spectroscopy, which can be used to gain insight into the polymer's chemical structure[25], [26] and can be used to classify polymer types. Due to their low reflectance of IR radiation and high fluorescence caused by the carbon black that lends them their dark colour, molding compounds unfortunately seem not to be a promising candidate for either technique. Additionally, these techniques offer only limited information about the inorganic constituents present in the form of filler particles and additives and are limited to analysis of the sample surface which may have structural and elemental deviations from the bulk material.

Techniques used traditionally for the analysis of the inorganic composition of solid materials, such as glow discharge mass spectrometry (GD-MS) and secondary ion mass spectrometry (SIMS) require conductive samples. As the polymer samples are non-conductive, the suitability of these techniques is limited.

Therefore, in this work, LIBS and Tandem LA-ICP-MS/LIBS are used for the comprehensive characterization and classification of mold compound samples. Laser induced breakdown spectroscopy (LIBS) is an uprising tool for polymer analysis and offers polymer specific information in the form of molecular emission lines, in conjunction with information about the main elemental constituents of polymers (C, H, N, O)[27]–[29]. The detection of minor inorganic constituents such as additives offers additional insights. Offering non-targeted analysis without the need to predefine the elements of interest, LIBS is widely applied for classification, discrimination, and identification studies (e.g., steel grades[27], iron ore samples[28] or ancient ceramics according to dynasty[29]). Additionally, offering fast multi-element analysis with simple instrumentation makes it a promising tool for quality assurance. For the detection of trace elemental constituents and impurities of the inorganic components of the material, LA-ICP-MS (Laser Ablation -inductively coupled plasma mass spectrometry) was employed in this work. To gain an overview and select relevant trace constituents for LA-ICP-MS analysis, liquid ICP-MS analysis was carried out beforehand.

Molding compounds from different suppliers are expected to show deviations in their elemental patterns resulting from different additives and base polymers used as well as contamination occurring during the manufacturing process. The identification of these variations should enable a differentiation of the samples. Batch to batch comparison during the chip manufacturer's production process could also help identify mix-ups. For this purpose data analysis is required, as the datasets collected by the instrumental measurements are too complex in their interpretation for a simple evaluation by hand.

Measurements from LIBS and Tandem LIBS/LA-ICP-MS were used for exploratory data analysis using different clustering methods to find differences and similarities between different types of molding compound and to visualize relationships amongst them. With the insights gained from exploratory data analysis, a random decision forest classifier was trained. For the classification of molding compounds, hand-picked emission lines were used as spectral descriptors for the LIBS spectrum, with the goal of improving the quality and stability of the model.

2 Theoretical aspects

2.1 Epoxy Molding Compound

Epoxy molding compounds, also known as epoxy mold compounds, are materials used for encapsulation of modern day electronic devices. Encapsulation improves handling during assembly and protects the sensitive semiconductor die, bond wires and lead frame against environmental influences such as shock, moisture and environmental contaminations. To optimally protect the device and to facilitate the molding process, molding compounds must have a number of special properties, such as a low thermal expansion coefficient (<10ppm/K[30]), high resistance against solder cracking, and good heat resistance, low moisture adsorption, low stress, and low melt viscosity[31].

The epoxy molding compounds used to achieve these goals consist of an eponymous epoxy resin, inorganic fillers such as fused silica or crystalline silica and additives to optimize workability during the molding process and to improve the properties of the finished product. Widely used additive include hardeners, accelerators, flexibilizers, flame-retardants, coupling agents, release agents, and pigments[31] [32].

Even though low moisture adsorption and low ion diffusion are desired properties of molding compounds, the encapsulated electronic devices cannot be considered hermetically sealed. The composition of the molding compound therefore has a direct influence on the risk of device failure due to corrosion or other failures. For example: chlorine ions originating from epichlorohydrin used for epoxidation as well as ions added as flame retardants such as antimony and bromine can accelerate the corrosion of bond pads and other metal surfaces of the device[23].

As the exact composition of an epoxy molding compound is generally a trade secret of the manufacturer, the prediction of long-term stability of the encapsulated device is limited by a lack of information.

2.2 Microwave assisted sample digestion

According to the Royal Society of Chemistry's "Chemical Methods Ontology", sample digestion is defined as:

> *"The decomposition of a sample into liquid form by treatment with enzymes or strong acids or alkalis."*[33]

For elemental analysis, the goal of digestion is to obtain an aqueous solution of the sample compatible with the analysis method. This includes the complete dissolution of the solid sample, removal of the organic matrix and conversion of inorganic compounds into an ionic form. For quantitative analysis, the loss of analytes due to formation of volatile compounds during digestion must be avoided. A comparable acid matrix for all samples, which allows for a high stability of ions in the solution and low background signals during measurement is advantageous if low limits of detection need to be achieved.

In conventional digestion procedures heating is performed using hot plates or heating blocks. The process is both time and labor intensive and offers only limited control over the internal temperature or pressure in closed reaction vessels.

The first use of an oscillating electromagnetic field for sample digestion was reported by Abu-Samra in 1975, who called his procedure using a modified kitchen microwave oven and open, glass Erlenmeyer flasks "wet ashing in a microwave oven". Advantages over digestions on a heating plate noted are the speed and safety of the method, as well as a reduced risk of air-borne sample contamination.[34]

Since then, microwave reaction systems for laboratory use have undergone continual development. Microwave assisted sample digestion has become routine particularly in the fields of geological and environmental analysis, as it is well suited for the digestion of soil and sediment samples containing both organic and inorganic substances such as silicates and oxides.

Modern-day microwave digestion systems for use in analytical laboratories still consist of one or more magnetrons connected to a cavity into which a rotor, containing the reaction vessels, is placed.

Instead of a single Erlenmeyer flask, multiple closed reaction vessels are utilized. Reaction vessels made of a pressure resistant outer body and a separate chemically resistant inner lining are in use as well as vessels that can be used without a liner. Vessels are made from a variety of materials, including but not limited to fibre reinforced polyether ether ketone (PEEK), polytetrafluoroethylene modified with perfluoropropylvinylether (PTFE-TFM) and aluminium oxide ceramics for the outer body and glass or PTFE-TFM for the liner. The reaction vessels are designed to withstand elevated internal pressures, some up to 20 bar, before built in safety features like the opening of a pressure valve or the rupturing of a burst disk prevent unsafe operating conditions. Elevated pressure and consequential higher boiling points allow for significantly faster digestion than open systems operating at ambient pressure.

To monitor temperature and pressure during the reaction, an immersive pressure and temperature probe inserted into a reference vessel can be used as well as piezoelectric pressure sensors integrated into the vessels and IR-temperature probes integrated into the rotor or the microwave cavity. In addition to IR-sensors, some rotors can be equipped with small magnetic stirrers to allow the content of the digestion vessels to be stirred during digestion.

The microwave reaction system is operated using an integrated PC to plan and execute digestion runs. Depending on the sensing equipment available, energy or temperature profiles are used. The oscillating electromagnetic field is produced by one or two magnetrons with a resulting maximum output level of up to 1500 W.[35] A ventilation system integrated into the microwave cavity prevents damage to the instrument due to the formation of corrosive gases during the digestion. As soon as the digestion is finished, the reaction vessels can be quickly cooled by a forced air cooling system.

Figure 2 shows the basic set up of a microwave digestion system, consisting of digestion vessels, a rotor and the computer controlled microwave cavity. Manufacturers offer a variety of accessories to facilitate the use of their microwave digestion systems for specialized techniques such as oxygen combustion, microwave assisted UV-digestion, drying, acid evaporation and protein hydrolysis.

In addition to the shorter reaction times and improved safety for the operator, the use of elevated pressure and temperature often also makes it possible to avoid harsh chemicals such as perchloric acid and reduces the amount of concentrated acids needed for complete digestion, making the digestion less expensive and more environmentally friendly.[36]

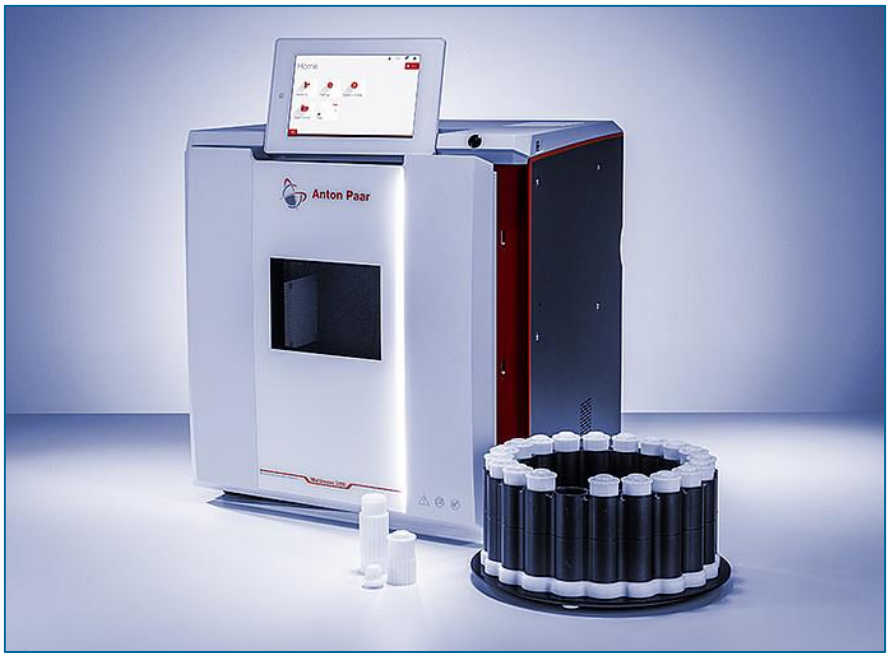

Figure 2: Image of a Multiwave 5000 microwave reaction system, showing the microwave cavity with integrated control computer, as well as the rotor outside of the cavity and PTFE-TFM reaction vessels.[37]

2.3 Inductively Coupled Plasma – Mass Spectrometry

In mass spectrometry, the mass to charge ratio of mono- or polyatomic ions is measured. Measurement methods can be classified by the type of charge, ionization or mass filtering method or the state of matter of the sample before measurement.

Ionization methods that produce ions of intact molecules and molecule fragments, both positively and negatively charged, are used in biochemical and organic analysis. These so-called “soft” ionization methods include Chemical Ionization (CI), Electrospray Ionization (ESI), Matrix Assisted Laser Desorption Ionization (MALDI) and Fast Atom Bombardment.

For elemental analysis, ionization methods that primarily produce positively charged monoatomic ions, such as secondary ionization (in secondary ion mass spectrometry, SIMS), glow discharge mass spectrometry (GD-MS), laser induced mass spectrometry (LIMS) and ionization in an inductively coupled plasma (ICP) are preferred.

Only inductively coupled plasma mass spectrometry (ICP-MS) is described further as it was the technique used for all mass spectrometry experiments performed within the context of this thesis.

2.3.1 Principle of analysis

Analyte in the form of droplets or small particles is carried by a gas stream into the hot zone of the ICP argon plasma torch where vaporization, atomization and ionization of the sample constituents takes place. The generated ions are accelerated toward a set of small cones that extracts ionized matter into the high vacuum part of the instrument in a collimated beam. Due to the expansion of the ion beam in the high vacuum, only a small fraction of all ions enters the mass analyser, where ions are separated according to their mass to charge ratio and finally reach the detector that records a mass spectrum.

2.3.2 Instrumental realization [38]

Although a variety of different configurations of ICP-MS optimised for different analytical questions and sample types are on the market, the general setup of an ICP-MS instrument for the measurement of liquid samples follows the same pattern illustrated in Figure 3.

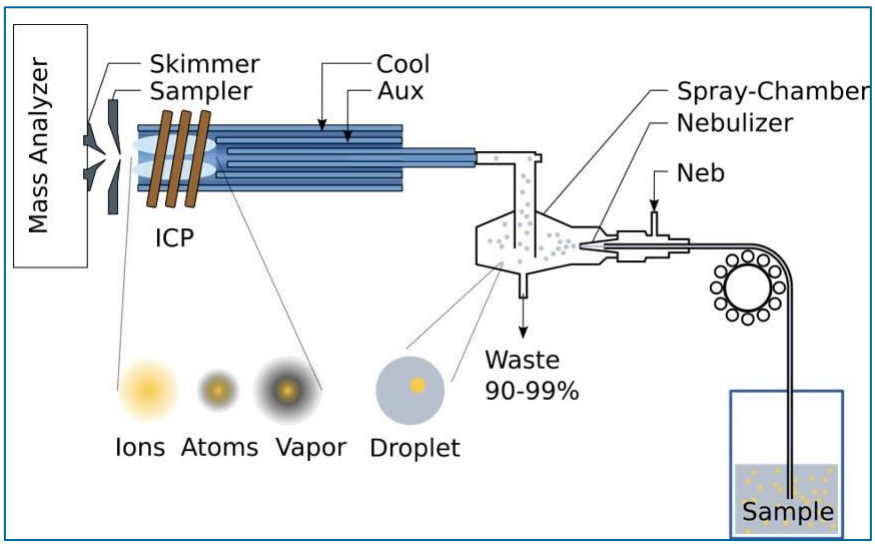

Figure 3: Schematic of a ICP-MS measurement system, adapted from [39].

2.3.2.1 Sample introduction: The nebulizer

Using a pump system, the sample solution is introduced into a pneumatic nebulizer equipped with a spray chamber, where argon is used as nebulizing gas to disperse the sample into fine droplets. Several different nebulizer geometries are in use, depending on the manufacturer of the instrument and the special requirements of the sample. The most common pneumatic nebulizers are known as Meinhard nebulizers.

The spray chamber is constructed in a way that the fluid dynamics within only allow the smallest droplets to be carried to the plasma torch, bigger droplets are discarded. For this reason, only 1-3 % of the sample solution reach the plasma torch, the remainder is drained from the spray chamber. Scott type and cyclonic spray chambers are most common.

2.3.2.2 Ionization: The ICP-Plasma torch and interface region

The plasma torch consists of 3 concentric tubes. The inner tube, called the injector tube, transports the sample from the nebulizer to the hot zone of the ICP plasma. Middle and outer tube carry argon gas, termed as auxiliary gas and cooling gas respectively. The gas flow from the nebulizer and the auxiliary gas flow allow the generation of an argon inductively coupled plasma by the ICP source, a coil that is placed concentrically around the upper end of the torch. The ICP source operates at frequencies of 27-40 Hz and a power of 1-2 kW. The cooling gas flow has the main purpose of protecting the torch from the high temperatures of the Ar-plasma.

The interface between the ICP torch operating at atmospheric pressure and the high vacuum part of the instrument consists of two to three metal cones with pinhole openings that allows the ionized matter to pass into the high vacuum part of the instrument in a collimated beam. An electromagnetic lens system is used to focus the ion beam.

2.3.2.3 Ion separation: the mass analyser

The purpose of the mass analyser is to separate the ions generated in the ion source according to their mass to charge ratio. This can be realised either spatially or temporally. The most widely used type of mass analyser in commercial ICP-MS instruments is the quadrupole mass analyser. ICP-MS instruments with time of flight analysers or double focussing sector field analysers for high mass resolution are also available. The combination of an ICP ion source with an ion trap mass analyser was described by Barinaga et al. in 1994 [40], and Milgram et al in 1997 [41], but is not commonly used.

2.3.2.3.1 Quadrupole mass analyser

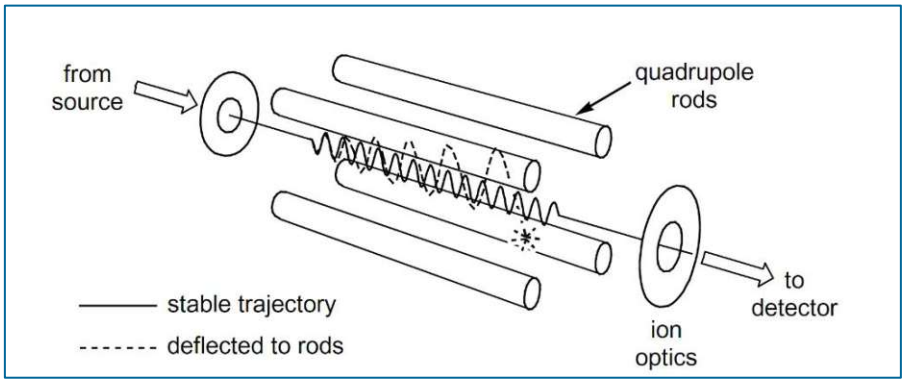

Figure 4: Quadrupole mass analyser, from [42].

First introduced in 1953 by Paul and Steinwedel [43], the quadrupole mass analyser consists of four cylindrical or hyperbolic rod-shaped electrodes, to which a voltage consisting of a dc and an ac component is applied.

Ions injected along the axis of the electrodes are subjected to an oscillating electrical field, which only allows ions fulfilling a resonance condition described by the Mathieu equation to pass through the mass filter to the ion detector.

Alternation of the voltage applied to the electrodes allows for the sequential selection of ions with different mass to charge ratios.

Quadrupoles can additionally be used as collision cells. The idea behind a collision cell is to remove polyatomic interferences of the same nominal mass as the analyte by having them collide with a nonreactive gas such as helium, which is introduced into the quadrupole. As the polyatomic interferences have a larger collision cross section compared to the analyte ions, their chance of collision with the gas are higher, making them statistically lose more energy. They are ultimately removed by an energy filter placed directly before the ion detection system[44].

The same principle is applied in reaction cells, with the difference that the inert collision gas is replaced by a reaction gas such as O_2 or CH_4 that selectively reacts with an interference. After the reaction, the interference has a different mass than the analyte and does not pass through the following mass analyser [44].

2.3.2.4 Ion detection

The ion detection system serves the purpose of registering the separated ions and securing that information. Today this is most often achieved by conversion into an electronic signal that is passed on to the data collection system. The detection system is located in the ultrahigh vacuum part of the instrument, after the mass analyser. The types of ion detection system that can be used depend on the type of mass analyser and on the ion currents to be detected.

For mass analysers that allow only ions of one mass to charge ratio to exit at one time, a single ion detector is suitable. For mass analysers that separate ions spatially, an array of multiple ion detectors can be used, as well as spatially resolved detectors such as photographic detectors or fluorescence screens.

The most common type of ion detector for Quadrupole ICP-MS instruments is the Secondary Electron Multiplier. It detects positively charged ions that impinge on its conversion dynode by amplifying the resulting electron current over multiple additional dynodes with increasingly positive potential. The electron collector registers a signal in the form of an electric current. Secondary electron multipliers can be operated either in current amplification or in ion counting mode, depending on the voltage applied to the dynodes. In current amplification mode, the output current can be amplified and measured by conventional techniques. In ion counting mode the use of pulse-counting electronics permits the detection of single ions. Disadvantages of secondary electron multipliers are the mass dependence of the amplification in current amplification mode and the dead time of the detector while a signal is processed [45].

To extend the linear detection range of the instrument, secondary electron multipliers are sometimes combined with a Faraday cup detector that is used for higher ion currents [45].

2.3.3 Advantages and disadvantages

ICP-MS is a very versatile elemental and isotope analysis technique suited for trace and ultra-trace analysis. It offers multi-element analysis after easy sample preparation and introduction for liquid samples with a dynamic range of 9-13 orders of magnitude, low detection limits (for most elements in the order of some ng/L), high precision and good accuracy[38]. Sample throughput of one to a few samples per minute, depending on analytical question and mass analyser used, allows rapid measurement of a large number of samples [38].

A disadvantage of the technique is the possible occurrence of interferences: polyatomic ions, doubly charged ions as well as isobaric singly charged ions overlap with the analyte ions in the mass spectra. Especially a large number of polyatomic ions containing Argon atoms makes measurement of certain elements and isotopes, such as $^{56}Fe^+$ (interferes with $^{40}Ar^{16}O^+$) and $^{40}Ca^+$ (interferes with $^{40}Ar^+$) difficult [38]. A possible way to overcome this problem is the use of a collision cell, where polyatomic ions can be removed. Another approach is the use of a high-resolution double focusing sector field mass analyser to differentiate between ions with the same nominal mass [46].

2.3.4 Direct measurement of solid samples: Laser ablation ICP-MS (LA-ICP-MS)

To measure solid samples directly, without the need for sample preparation, a laser ablation device can be coupled with the mass spectrometer. For this purpose, a laser ablation chamber is connected to the MS instrument instead of the nebulizer and spray chamber, as illustrated in Figure 5. A pulsed laser is focussed on the sample surface and repeatedly fired to ablate a small amount of material from the sample surface. A gas flow (He or Ar) transports the ablated material from the ablation chamber to the ICP torch.

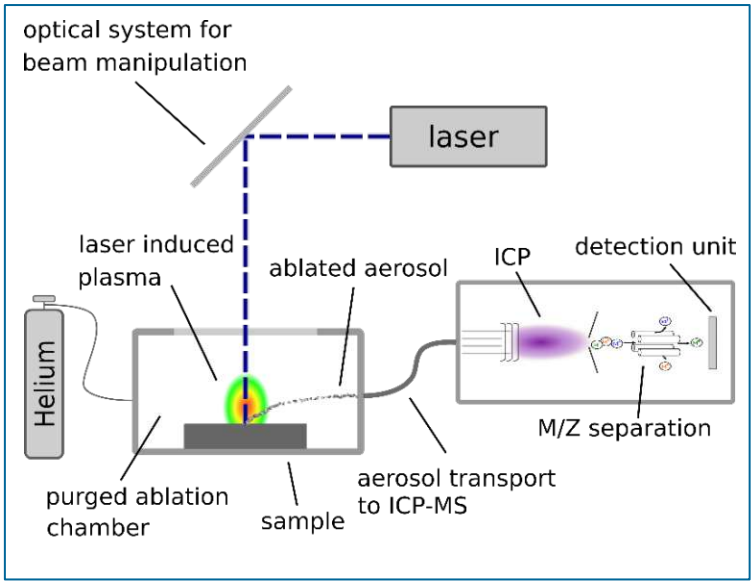

Figure 5: Schematic of a LA-ICP-MS instrument.

The advantage of LA-ICP-MS is the direct measurement of solid samples, allowing spatially resolved measurements and avoiding time and labour-intensive sample preparation as well as minimizing the risk of contaminating the sample.

The disadvantage of direct measurement of solid samples is the more complex problem of quantification. The recorded intensities are influenced by the ablation efficiency as well as by the transportation efficiency for different particles, resulting in fractionation effects. Matrix matched standards for solid samples, especially for novel or not commonly used materials are often not available.

2.4 Laser principles

The word “laser” is originally an acronym for “Light Amplification by Stimulated Emission of Radiation” [47].

Based on its generation principle, the light emitted from a laser has some remarkable properties, such as high spatial convergence, monochromaticity and coherency as well as low beam divergence, making it especially suitable for applications in analytical instruments[48].

Every laser possesses an active medium, a means to induce population inversion in the active medium by optical pumping and a feedback system, also called optical resonator [49].

2.4.1 Active medium

The active medium is a collection of atoms of molecules, for which a population inversion of two energy states can be achieved ($N_j > N_i$ for $E_j > E_i$). It can be gaseous, liquid or solid. The difference in energy between the inverted energy states determines the fundamental wavelength of the laser [49].

2.4.2 Laser pumping

Under normal circumstances, the distribution of atomic energy state populations follows Boltzmann’s principle[49].

$$\frac{N_j}{N_i} = e^{-\Delta E_{ji}/kT} \qquad \text{for } E_j > E_i$$

To achieve the population inversion necessary for laser action, $N_j > N_i$, an external energy source must be used to excite the active medium to a non thermal equilibrium distribution. Different methods of pumping are employed in

different types of laser-systems: commonly used are optical pumping methods using a flash lamp, diode stack or second laser. For semiconductor lasers, electrical pumping is used [49].

2.4.3 Optical resonator

With each pass through the active medium, the light beam is amplified. To achieve high intensities, the active medium is placed inside an optical resonator to increase the interaction length between the light beam and the active medium. The dimensions of the optical resonator determine the modes (axial and longitudinal-traverse mode frequencies) of the laser [49].

2.4.4 Diode pumped Nd:YAG Laser

For most LIBS and many laser ablation applications, a flash lamp or diode pumped Nd:YAG laser is used [48]. The Nd^{3+} ions doped into an Yttrium Aluminium Garnet (YAG) crystal matrix serve as active medium. A flashlamp or diode stack is used for optical pumping. To achieve a high population inversion an electro-optic Q-switch is placed inside the optical cavity. It prevents the premature start of stimulated emission by absorbing photons of the laser wavelength until it is activated and becomes transparent [49]. The Q-switched pulse emitted by a Nd:YAG laser has a duration of 5-10 ns [48]. The Nd:YAG laser has a fundamental wavelength of 1064 nm, situated in the infrared region of the optical spectrum.

By passing the laser pulse through a birefringent material such as potassium dihydrogen phosphate (KDP), the frequency of the laser pulse can be multiplied. The resulting harmonic wavelengths at 532 nm (first harmonic), 266 nm (forth harmonic) and 213 nm (fifth harmonic) are then used for LIBS or laser ablation imaging applications.

2.5 Laser Induced Breakdown Spectroscopy

LIBS is an acronym for laser induced breakdown spectroscopy. A laser is used to ablate, atomize and excite a small amount of sample. Excited ionic and atomic species emit light with characteristic wavelengths that can be used for qualitative and quantitative characterization of the sample.

A LIBS instrument consists of a sample chamber, a laser system, optical systems to focus laser beam and collect the light emitted by the sample plasma and a detection system connected to a computer controlling the instrument. Figure 6 shows the typical setup for a LIBS instrument. For stand-off LIBS applications, the laser beam is focused on a sample outside of the instrument using the optical system.

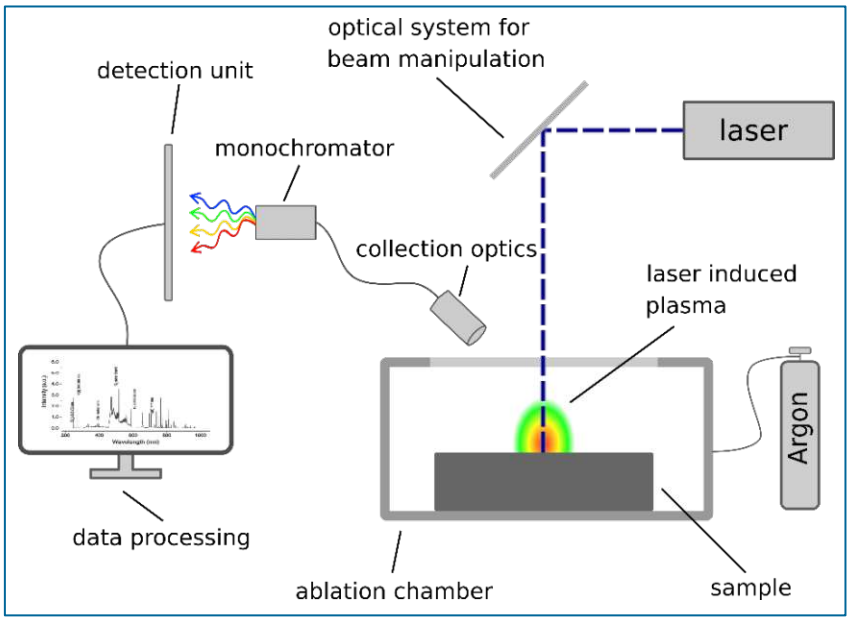

Figure 6: Typical setup for LIBS measurement.

2.5.1 Optical system

To focus the laser pulse on the sample, one or multiple lenses or mirrors are used. Typically, spherically symmetric optical elements are used to generate a circular laser spot on the sample. A second set of optical components is used to collect the light emitted by the LIBS plasma. To direct the collected light to the detection systems, fiberoptic cables are used.

2.5.2 Detector

The task of the detection system is to record a spectrum of the radiation emitted by the LIBS plasma. For this purpose the polychromatic light emitted by the plasma has to be separated by wavelength using a spectrograph. Spectrographs rely on a combination of dispersive elements such as gratings and prisms to separate the light according to wavelength. The most commonly used spectrographs for LIBS are Czerny-Turner and Echelle spectrographs in combination with diode array detectors or a CCD [48]. The wavelength resolution of the LIBS spectrum depends on the dispersive element and the detector used.

2.5.3 Advantages and disadvantages

LIBS permits direct analysis of solid samples, making it a useful tool for material characterisation. As all emission lines from the sample are detected at the same time, LIBS allows for simultaneous and non-targeted multi-element analysis. The capability to detect Hydrogen, Oxygen as well as small organic fragments of Organic molecules such as C_2 and CN in make it very useful for the analysis of organic materials such as synthetic polymers. Moreover,

LIBS is perfectly suited for the investigation of composites consisting of organic and inorganic materials, such as epoxy molding compounds. The LIBS setup also permits imaging and depth profiling.

LIBS can be used routinely for the analysis of major and minor constituents with some elements even showing LODs in the low ppm range. The lateral resolution of up to some micrometres and the surface selectivity of the method allows elemental mapping and depth profiling. Due to the great influence the surface structure and sample matrix have on the plasma generation and sample excitation process, quantitative analysis is difficult without matrix matched calibration standards.

2.6 Tandem LA-ICP-MS/LIBS

To combine the simultaneous multi-element analysis of LIBS with the trace analysis capability of LA-ICP-MS, a Tandem measurement concurrently detecting emission spectrum and ion intensities from the same sample region can be performed. The instrumentation for Tandem LA-ICP-MS/LIBS is a combination of both setups. A LIBS detection system records the emission spectrum originating from the plasma generated by the laser, while the sample aerosol is transported to the mass spectrometer. The setup is illustrated in Figure 7. As the optimal operating conditions regarding Laser intensity, type of chamber gas and inert gas flow differ between the two techniques, optimisation to find the best compromise condition is required.

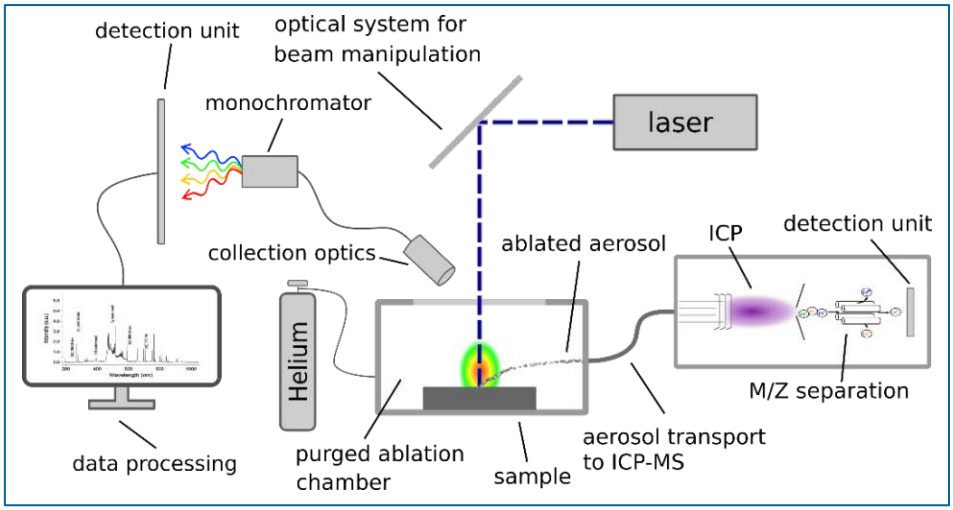

Figure 7: Setup for Tandem LA-ICP-MS/LIBS measurements.

2.7 Multivariate Analysis

According to the DIN norm ISO 18115-1[50], defining vocabulary for surface chemical analysis, multivariate analysis is defined as

> *"analysis involving a simultaneous statistical procedure for two or more dependent variables".*

According to the norm, multivariate analysis summarizes data containing many different statistical variables using a smaller number of variables, thus simplifying it and making it more understandable.

For the purpose of multivariate analysis, data from measurements is organised in the form of a data matrix. Each column corresponds to a measured variable, for example the intensity of emission at a certain wavelength in a LIBS spectrum. The results of the measurements of each sample are recorded in a row of the matrix. For m measurements and n properties, the data matrix is of size $m \times n$.

For experiments making use of multivariate analysis, a common work flow can look as follows:

1. Collection of measurement data
2. Data pre-processing
3. Performance of data analysis procedures
4. Interpretation of analysis results

Multivariate data analysis techniques have been used in a variety of fields for data reduction, pattern recognition, cluster analysis, classification and quantification of data. The application of multivariate analysis to data obtained by chemical measurements and/or to answer questions associated with the field of chemistry is also termed "chemometrics" [48].

2.7.1 Data collection

The measurement of data intended for multivariate analysis is performed in the same manner as the respective measurements would normally be conducted. It is important to note that only data of good quality can lead to good results, information that has not been collected in data measurement cannot be found using multivariate analysis. For that reason, it is important to produce initial measurement data of the highest possible quality. Therefore, optimization of measurement conditions is recommended prior to analysis.

2.7.2 Data preprocessing

According to DIN ISO 18155, data pre-processing refers to

> *"[the] manipulation of raw data prior to a specified data analysis treatment".*

The term includes the selection of variables as well as transformations applied to the data matrix. Data pre-processing procedures are intended to improve the meaningfulness and interpretability of the results of following data analysis procedures. Care must be taken not to distort the data in a way that may lead to erroneous conclusions based on artefacts caused by the data pre-processing.

2.7.2.1 Data normalisation

Data normalisation is employed to correct for changes in signal intensity between measurements. If an internal standard is available, all measured signal intensities are divided by the intensity of the internal standard. If no internal standard is available for this intensity correction, an alternative approach is to normalise each matrix row by its standard deviation and centre it to a mean of 0.

2.7.2.2 Variable selection

Some measurement data contains a large number of variables and sometimes a high amount of collinearity, for example spectra generated by IR-spectroscopy or LIBS. The selection of a reduced set of variables is often beneficial for multiple reasons.

From a data-science point of view, the data matrix represents a multi-dimensional data space. Each variable adds a dimension to the space, while each measurement is represented by a single point. A data matrix of size $m \times n$ corresponds to m points in a n dimensional space. Pattern recognition methods show the Hughes phenomenon: The performance of a pattern recognizer for a given number of measurements improves with the number of variables, until a peak is reached, after which additional variables cause the performance to deteriorate again [51]. The corollary for the application of multivariate statistics to a set with a fixed number of samples is that the number of variables used for data analysis has an optimum that should not be exceeded.

With the number of dimensions, the demands on computational time and memory for the performance of analysis procedures also increase, often exponentially, depending on the specific algorithm. This makes the calculation expensive in time and resources [52].

More obvious from a chemical standpoint is the fact that the exclusion of spectral regions that do not contain signals relevant to the sample will reduce the amount of noise included in the dataset. The combination of multiple data points along the curve of a single spectral feature can also improve the signal to noise ratio and is standard practice in the evaluation of emission spectra. The variables generated based on chemical considerations out of a measured spectrum are also called “spectral descriptors” in literature [52].

2.7.2.3 Data transformation

DIN ISO 18155-1 defines transformation as

> *“procedure in which each element in the data matrix is transformed by a defined function”.*

Some examples for data transformation are the taking the logarithm or the square root of each value. More commonly, data is transformed using different linear functions, also referred to as scaling or centering.

2.7.2.3.1 Data scaling

According to DIN ISO 18155-1, data scaling is

> *“[a] procedure in which the data matrix is divided element-wise by a scaling matrix”*

Scaling procedures can be applied prior to or after variable selection. Depending on the nature of the scaling matrix, we refer to normalisation or variance scaling, amongst others.

For **normalisation** of data as described in 2.7.2.1, the scaling matrix consists of a constant for each sample (matrix row). Normalisation is often applied to the complete dataset before variable selection is performed.

The scaling matrix for **variance scaling** contains the standard deviation of each variable across all samples (matrix column). It equalises the importance of all variables for multivariate analysis methods.

Mean centering is performed after variable selection and data scaling. Each value is transformed by subtraction of the column mean. Mean centering emphasises the difference between measurements instead of the difference of a single measurement to the origin.[50]

The combination of variance scaling and mean centering is termed *auto scaling* in DIN ISO 18155-1. In other sources, the designation **standardisation** is used, as the resulting data column has a mean of 0 and a standard deviation of 1[53].

2.7.3 Data analysis methods

Multivariate data analysis methods can be split into two distinct groups. Unsupervised methods only rely on the data matrix. They are used for descriptive purposes, to find similarities and differences between different samples and the responsible variables. Supervised methods are used for predictive purposes.[54] For the model generation, a set of samples with known target values is needed. The model is then applied to a new set of samples to predict the target value. In the following paragraphs, the unsupervised and supervised methods used in this thesis are introduced.

2.7.3.1 Unsupervised methods

2.7.3.1.1 Principal component analysis (PCA)

Principal component analysis is a form of factor analysis. In factor analysis, the data matrix X is decomposed into the scores matrix T and the transpose loadings matrix P'. If factor analysis is used for dimensionality reduction, the number of factors selected is smaller than the rank of the data matrix and the decomposition includes a residual matrix E[50], assumed to contain noise.

$$X = TP' + E$$

The transformation is equivalent to a rotation of the data space, with the factors acting as new coordinate system. Each factor is associated with a column in the loadings and scores matrix. The rotation of the data space is illustrated in Figure 8.

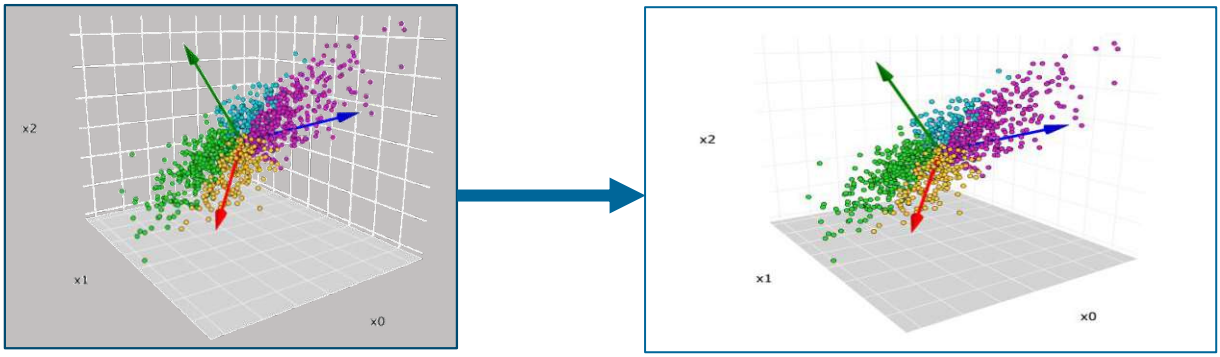

Figure 8: Illustration of the rotation of the data space for PCA, adapted from[55].

In Principal Component Analysis, the rotation maintains orthogonality. The factors are eigenvectors of $X^{-1}X$, sorted in descending order according to their corresponding eigenvalues and called principal components [50].

The result of a PCA can be used to find clusters in data and to visualise differences between samples. Based on the generation mechanism of the PCA, the result is highly sensitive to scaling. Variables with high total values have a stronger impact than those with low values. For this reason, scaled variables are recommended when using PCA.

The results of a PCA can be displayed in the form of score-score plots, which are the projection of the multidimensional space to the plane generated by two principal components. A bi-plot combines the score-score plot with the projection of the original coordinate system and is helpful for the visualisation of the influence of certain descriptors on the principal components.

2.7.3.1.2 Hierarchical cluster analysis

Hierarchical clustering methods construct clusters by recursively partitioning the data. The result is a dendrogram, representing the similarity levels of individual datapoints and clusters. To obtain clusters, the dendrogram is cut at the desired similarity level. Two general approaches can be distinguished[54]. This is also illustrated in Figure 9.

1. Agglomerative clustering: Each datapoint starts out as an individual cluster, clusters are merged.
2. Divisive clustering: all data belongs to one original cluster that is divided into subclusters.

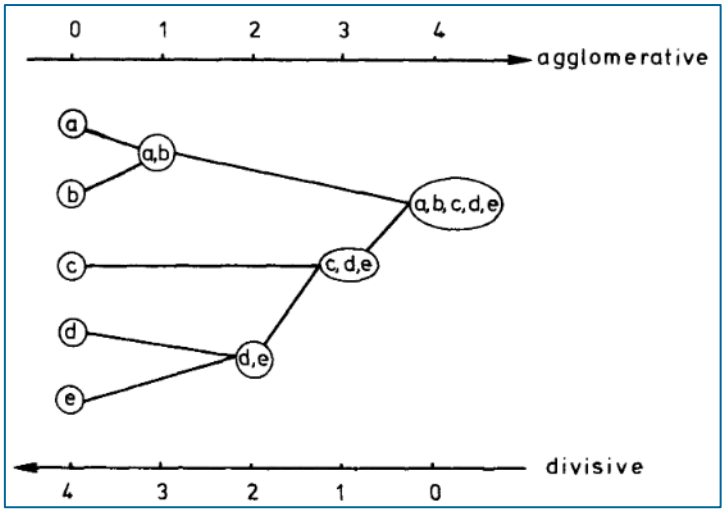

Figure 9: Illustration of agglomerative and divisive hierarchical clustering methods, from[56].

For merging or division of clusters, a distance measure is necessary. The distance measure indicates the similarity between two datapoints. Useful distance measures should be symmetrical, and zero for the distance of identical datapoints. Commonly used distance measures for numeric attributes are the *Euclidian distance* and *Manhattan distance*[54]. In case of differently scaled attributes, standardisation before clustering is helpful to ensure that all attributes have equal influence on the clustering result.

Single link clustering takes the distance between the closest members of two clusters as the distance between clusters. The clusters with the shortest distance are merged. A related approach is **complete-link clustering**, which uses the largest distance between members of two clusters. For **average-link clustering**, the average distance between members of two clusters is used [54].

Wards method is another agglomerative clustering method. The clusters for merging are chosen in a way that minimises an objective function, most commonly the variance, of clusters being merged[57].

2.7.3.2 Supervised methods

Supervised methods are used to build classifiers or regressors that can be applied to new data with unknown target values. Classifiers match each sample to one of a number of discrete classes, while regressors predict the value of a continuous quantity of the sample. For example, predicting the nationality of a person would be a task for a classifier, whereas a regressor would be better suited for predicting their age. Only classifiers are discussed further, as regressors are not applied in this work.

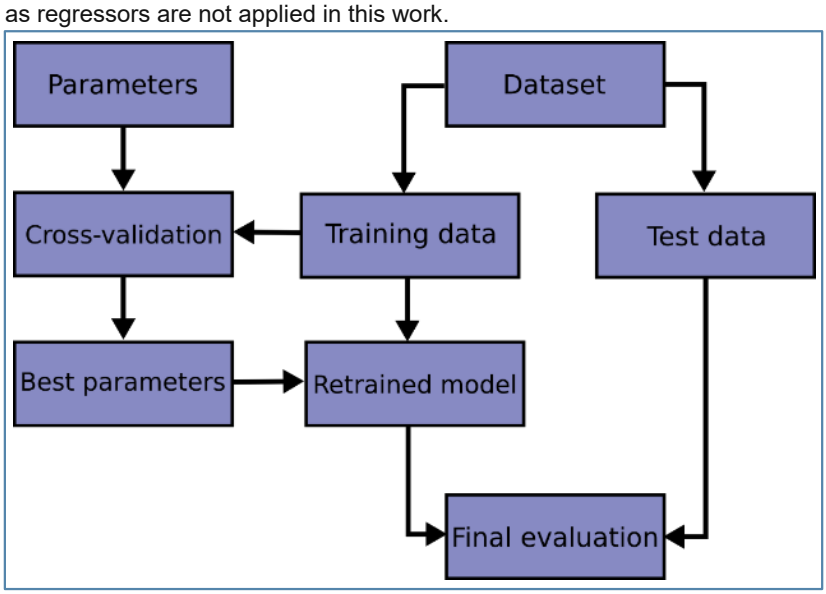

Figure 10: Typical workflow for the generation and optimization of a supervised model.[58]

Figure 10 illustrates the typical workflow for the generation of a supervised classification model. The available dataset of samples of known class is split into a training and a test dataset. The split proportion is dependent on the absolute size of the dataset. The test dataset is held back and only used for the final performance validation of the developed classification model, all intermediate model development steps are performed using only the training data.

The training data is used to optimize the parameters of the classification method. These parameters are sometimes also called “hyperparameters”, to distinguish them from the model parameters that are generated during model training. For cross-validation, the training data is again split, with one part of the data being held back from model training and used as test data for performance evaluation. This process is repeated multiple times for each set of hyperparameters under investigation, to find the optimal set of hyperparameters. The splitting of the dataset is necessary to ensure that the model does not achieve a good performance by simply memorizing the data. Such a model would perform well on the training data but poorly on independent test data, which is called overfitting.

The best hyperparameters are then used to train the optimized model using all data from the training dataset. This final model is ultimately evaluated using the test data. If the performance of the model is satisfactory, it can then be applied to new data with unknown target class.

2.7.3.2.1 Decision tree

A decision tree is a classifier that consists of a root node and multiple branch and leaf nodes. Leaf nodes contain a sample class or class distribution, whereas branch nodes and the root node contain a splitting rule, consisting of a sample attribute and a splitting value.

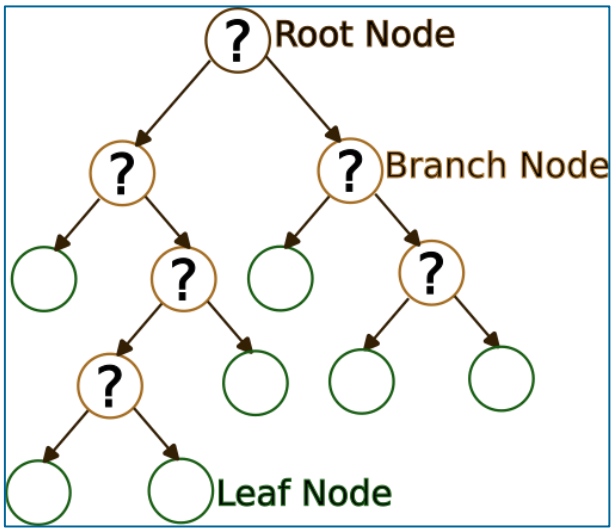

Figure 11: Sketch of a decision tree.

In construction of a decision tree, branch nodes are selected in a way that minimises the disorder in the training set. Different measures for the decrease in disorder are in use. Some commonly used impurity functions to determine the best split are *gini* and *entropy* [59].

For more complex datasets, decision trees are prone to memorizing the training data. This overfitting can be reduced by removing some branches, also called “pruning of the tree”, which is done using a validation set.[60]

To use a decision tree to classify a sample, the path from the root node to a leaf node is followed. At the root node and each branch node, a decision is made based on a sample attribute. The class of the located leaf node is then assigned to the sample.

The structure of decision trees is intuitively accessible to humans. They allow to draw conclusions about the influence of different sample attributes on the classification by simply looking at the branch nodes.

2.7.3.2.2 Random decision forest (RDF)

The Random decision forest classification method originates from the field of machine learning. It is an ensemble classification method based on the decision tree classifier.[61]

The construction of a random forest classifier is illustrated in Figure 12. For the random forest classifier, the training data is partitioned into random subsets of samples of equal distribution. A decision tree is built from each subset. For each split, only a random subset of sample attributes is considered. All trees together form the random forest. When a random forest classifier is used for classification, the new item is classified independently by each tree. The results are then merged by majority voting or averaging over each trees probabilistic prediction to obtain the final classification.[62]

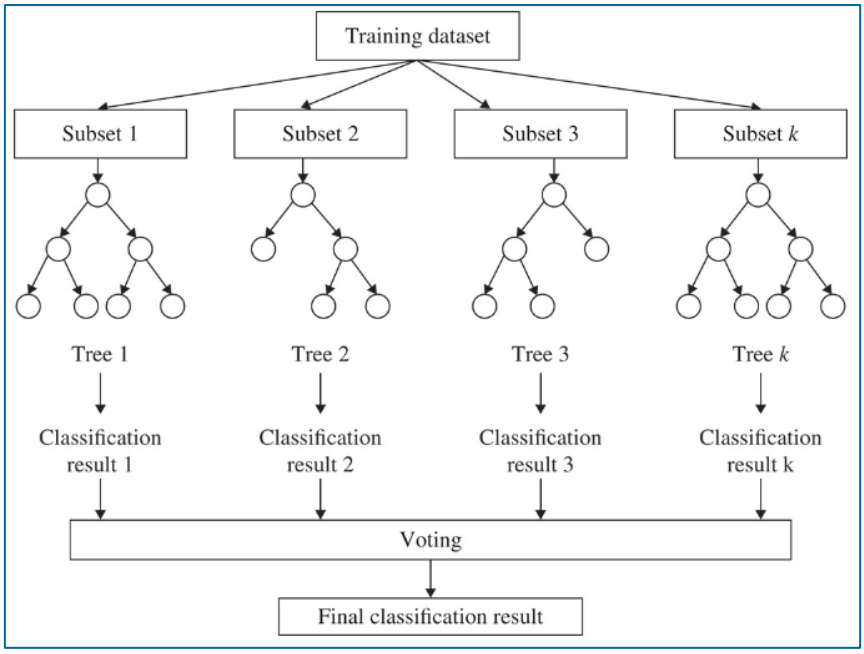

Figure 12: Illustration of the training and application process of a random decision forest classifier, from[63].

A random forest model is of higher complexity than a single decision tree and less understandable to human minds. To gain insight into the model, the importance of individual sample attributes can be calculated, based on their contribution to the decrease in impurity to each tree.

3 Methods

3.1 Samples

To generate data for the development of a classification model, 29 samples of 20 commercially available molding compounds sold by 4 different manufacturers (A, B, C, D) were analysed. Different types of samples were used for different mold compounds (tiles, packages, and molding culls, as shown in Figure 13). For some molding compound types multiple sample types were obtained (e.g. tile and package for A1).

Table 1: List of all sample designations and their respective sample types.

Designation	type of sample	Designation	type of sample	Designation	type of sample
A1	tile, package	B1	tile, package	D1	tile,cull
A2	tile	B2	tile	D2	tile,cull
A3	tile, cull	B3	tile, package	D3	cull
A4	tile	C1	tile, cull	D4	cull
A5	cull	C2	cull	D5	cull
A6	cull	C3	cull		
A7	cull	C4	cull		
A8	cull				

All samples (molding culls, tiles and complete semiconductor packages) underwent LA-ICP-MS and LIBS analysis. The 10 molding compound samples available in the form of 34 x 34 x 1.5 mm tiles were broken up and used for digestion and liquid ICP-MS measurement as well as embedded in epoxy resin and polished for SEM imaging.

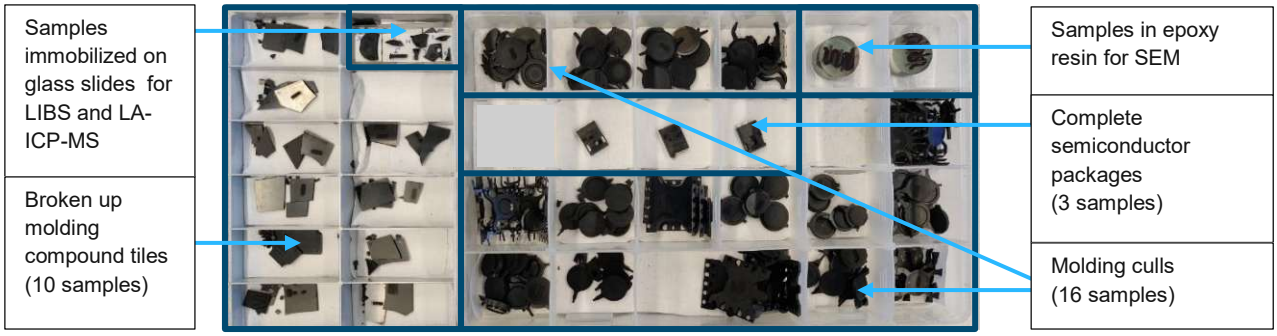

Figure 13: Depiction of all molding compound samples investigated.

3.2 Sample preparation for ICP-MS measurement

Digestion of 10 Molding compound samples was carried out using an Anton Paar Multiwave 500 Microwave reaction system equipped with a 20SVT50 rotor and 50 mL PTFE-TEM digestion vessels. For each sample, 5 digestions were carried out. 2 blank digestions were performed during each digestion run, totalling 12 digestion vessels in the rotor at a time. Additional blank values of all digestion vessels were collected by performing “digestions without sample” in between each digestion run under the same operating conditions.

A small piece of molding compound (20-30 mg) was added to 3 mL of 65 % HNO_3 (Merck, EMSURE®,p.a.) and 0.2 mL of 40 % HF (Merck, SUPRAPURE®,p.a.) in a digestion vessel. After closing, the digestion vessels were placed in the rotor of the microwave digestion system and heated according to the temperature program detailed in Table 2 and illustrated in Figure 14 (a).

Table 2: Temperature program for microwave digestion.

Program step	**time**
Heating from room temperature to 185 °C	20 min
Holding the temperature at 185 °C	15 min
Cooling to 70 °C as fast as possible	ca. 17 min

Figure 14 (b) shows the temperature profile of the 12 reaction vessels during a digestion run as measured by the IR temperature probe. The lines in the lower third of the diagram correspond to the 8 empty slots of the 20 position rotor. The difference in maximum temperature between the hottest (220 °C) and coolest (156 °C) vessel is being attributed to tensions in the vessel material and lead to the loss of up to one third of the digestion volume in the hottest vessels.

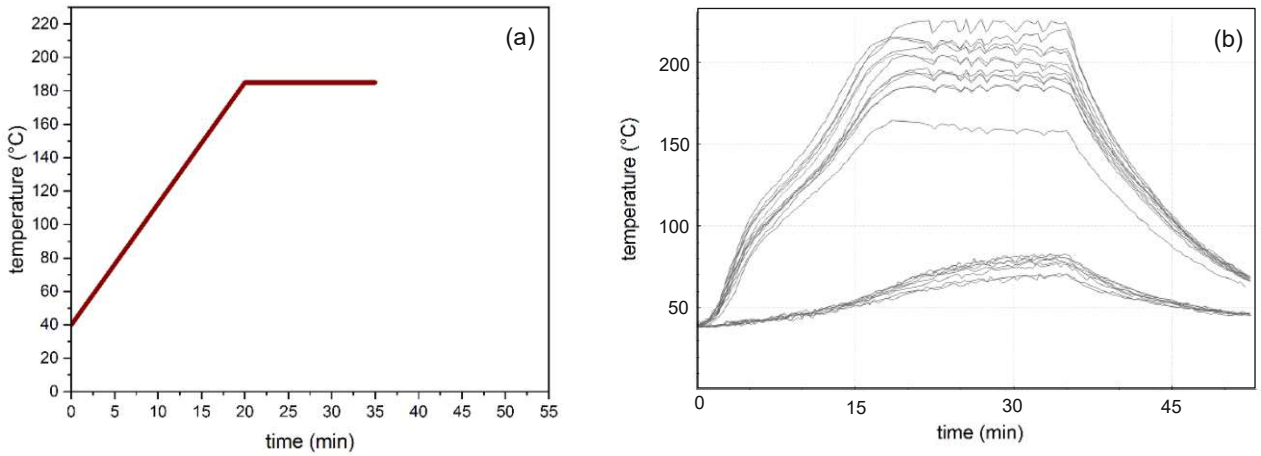

Figure 14: (a) Temperature program during microwave digestion. (b) IR-Temperature measurements of digestion vessels. The curves in the lower third of the diagram correspond to empty spots in the rotor.

The reaction vessels were taken out of the rotor and left to cool to room temperature (20 °C) in the fume hood before opening.

The cooled solutions were transferred to 15 mL polypropylene centrifuge tubes, filled to 3 mL with conc. HNO_3 to compensate for loss of volume due to different venting behaviour of the digestion vessels and diluted with deionized water (Thermo Scientific EASYPURE II, 18.2 MΩ) to a total volume of 12 mL.

For ICP-MS measurement, two dilutions with a volume of 9 mL were prepared from each of the sample digestions. This was achieved by volumetrically diluting the sample digests with 0.65 % HNO_3 by a factor 10 and 100 respectively. From the blank digestions, only the factor 10 dilution was prepared. 1 µg/L of Indium was added to all dilutions to act as internal standard.

All sample preparation steps were tracked gravimetrically using an analytical balance (Satorius, Entris 124I-1S), to determine the weight ratio of used solid molding compound sample to the measured diluted solution.

3.3 Preparation of a standard series

To allow quantitation of different elements in the digested sample solutions, two separate standard series were prepared by diluting standard solutions with 0.65 % HNO_3. The following Table 3 lists the utilized certified multi- and single element standard solutions and the concentration range of the standard series for all measured elements. Like the sample solutions, each dilution step was tracked gravimetrically and the standard dilutions were enriched with 1 ppb indium as internal standard.

Table 3: Standard series for ICP-MS measurement.

series	conc. Range	Elements	Standard solutions
1	0.9 pg/g - 45.8 ng/g	Li, Be, B, Na, Mg, Al, K, Ca, Cr, Mn, Fe, Ni, Co, Cu, Zn, Ga, Sr, Cd, Te, Ba, Tl, Pb, Bi	Certipur® ICP multi-element standard solution VII (24 elements in dilute nitric acid), Merck
2	0.1 pg/g - 0.5 ng/g	Sn	Certipur® Tin ICP standard, traceable to SRM from NIST $SnCl_4$ in HCl 7%, Sigma Aldrich
		Sb	Antimony ICP standard traceable to SRM from NIST Sb_2O_3 in HCl 7%, Merck
		Nd	ICP multi-Element standard Aristar®, BDH
		Pr	Praseodymium Plasma Emission Standard (ICP-MS), VWR
	0.5 pg/g - 2.5 ng/g	Ce	Cerium, plasma standard solution, Specpure® Ce in 5 % H_2O, Alfa Aesar
		La	Lanthanum plasma emission standard(ICP), VWR
		Ba	Certipur® Barium ICP standard, traceable to SRM from NIST Ba(NO3)2 in HNO_3 2-3 %, Merck
	0.9 pg/g - 4.9 ng/g	W	Certipur® Wolfram ICP standard, traceable to SRM from NIST $(NH_4)_2WO_4$ in H_2O, Merck
		Hf	Hafnium plasma standard solution, Specpure®, Alfa Aesar

3.4 ICP-MS measurement of digested samples

The diluted samples and standard solutions were measured using a ThermoFisher iCAP Q quadrupole ICP-MS (Thermo Fisher Scientific) with Ni-alloy cones equipped with a Meinhard Nebulizer and cyclonic spray chamber. Measurement parameters are listed in the following Table 4.

Table 4: ICP-MS measurement conditions for digested samples.

Plasma RF power	1550 W
Dwell time per isotope	10 ms
Sample flow rate	400 µl/min
Nebuliser gas flow	1 l min^{-1}
Coolant gas flow	14 l min^{-1}
Auxiliary gas flow	0.8 l min^{-1}
Main runs	3
Measurement mode	KED mode (gas: 10 % O_2 in He, 2.7 ml min^{-1})
Measured Isotopes	^{7}Li, ^{9}Be, ^{11}B, ^{23}Na, ^{24}Mg, ^{27}Al, ^{39}K, ^{44}Ca, ^{50}Cr, ^{52}Cr, ^{55}Mn, ^{57}Fe, ^{58}Ni, ^{59}Co, ^{60}Ni, ^{63}Cu, ^{65}Cu, ^{66}Zn, ^{68}Zn, ^{69}Ga, ^{71}Ga, ^{86}Sr, ^{88}Sr, ^{111}Cd, ^{112}Cd, (^{115}In as internal Standard), ^{118}Sn, ^{120}Sn, ^{121}Sb, ^{125}Te, ^{126}Te, ^{137}Ba, ^{138}Ba, ^{139}La, ^{140}Ce, ^{141}Pr, ^{142}Ce, ^{143}Nd, ^{146}Nd, ^{178}Hf, ^{182}W, ^{184}W, ^{203}Tl, ^{205}Tl, ^{207}Pb, ^{208}Pb, ^{209}Bi

Three replicate measurements of each solution were recorded, resulting in 15 datapoints per sample and isotope for the 100x as well as for the 10x dilution. Measurements of the blank digestions were used to determine background concentration caused by the reagents and digestion vessels. The Indium signal was used as internal standard to correct for instrument drift.

The calibration curves constructed from the measurement of the standard solutions for selected elements are shown in Figure 15. Standards that produced a signal significantly higher than the highest signal measured from a sample were excluded. The derived RSDs were in the order of 1-10 %, inversely correlating with the standard concentration. Figure 15 shows a linear correlation between measured signal intensities and known standard concentrations. The linear calibration achieved correlation coefficients above 0.9998 for the investigated elements.

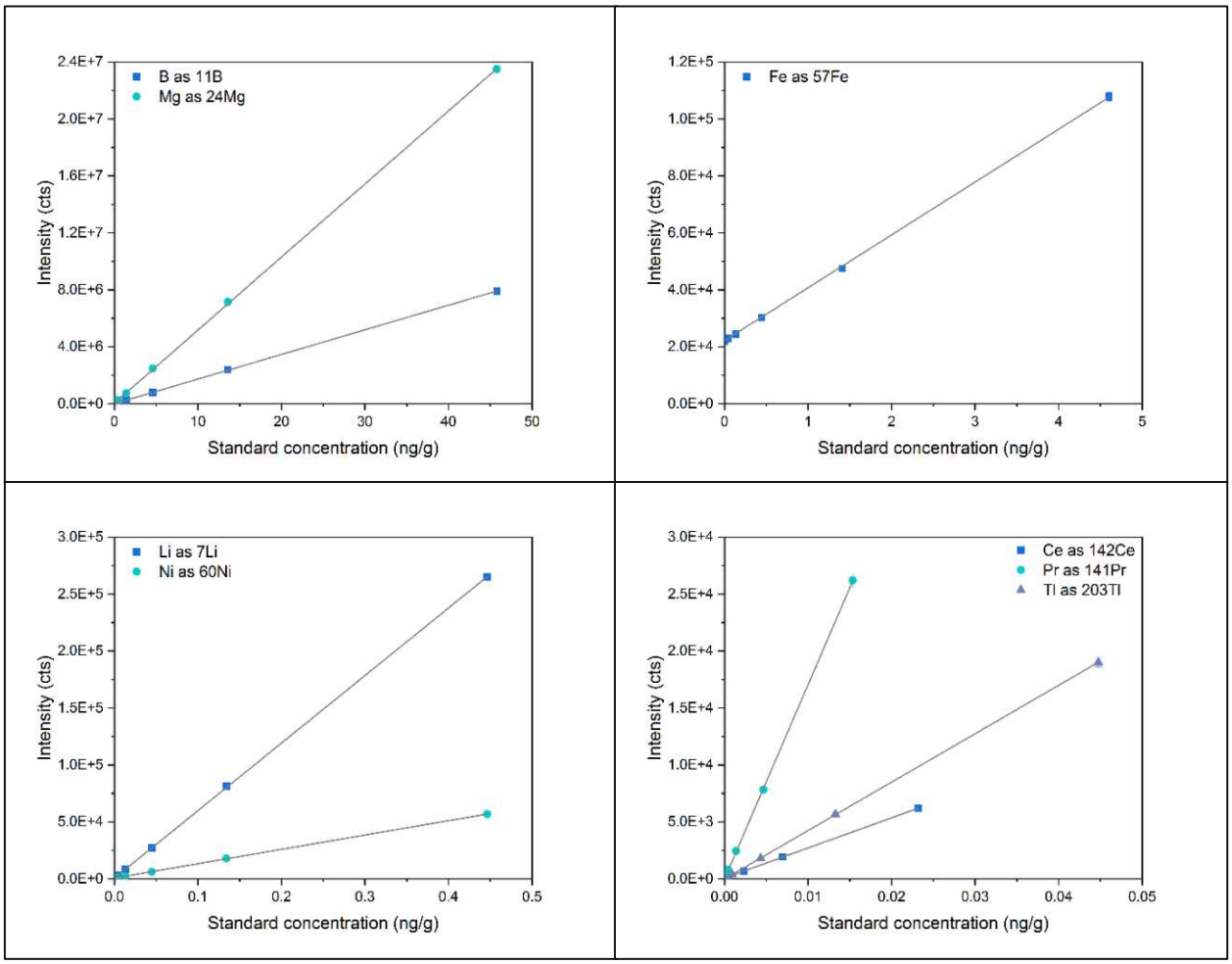

Figure 15: Selected calibration curves for liquid ICP-MS measurement.

3.5 LA-ICP-MS measurement

For LA-ICP-MS measurement, a small piece of each molding compound sample was broken off and fixed to a microscope glass slide using double sided tape. The sample slides were placed in the sample chamber of the laser (213 esi, New Wave Research). The laser ablation system was connected to the ICP-MS using flexible PTFE tubing with an internal diameter of 1.5 mm. To remove surface contaminations, a preablation was performed before the measurement. The following Table 5 and Table 6 list the measurement conditions used for the laser and the MS instrument (iCAP Q, ThermoFisher). For LA-ICP-MS analysis, 10 parallel line scans with a length of 1 mm were ablated. Each line was divided into five equal sections. Transient signals from each of the 50 sections were averaged and used as a variable for further data evaluation. Therefore, 50 datapoints per sample were obtained.

Table 5: Mass spectrometer settings used for LA-ICP-MS.

Plasma RF power	1550 W
Dwell time per isotope	10 ms
Coolant gas flow	14 l min^{-1}

Auxiliary gas flow	0.8 l min^{-1}
Ar make-up flow	0.8 l min^{-1}
He gas flow in ablation chamber	0.5 l min^{-1}
Measured Isotopes:	^{10}B, ^{25}Mg, ^{34}S, ^{53}Cr, ^{55}Mn, ^{56}Fe, ^{59}Co, ^{60}Ni, ^{63}Cu, ^{71}Ga, ^{121}Sb, ^{140}Ce, ^{141}Pr, ^{146}Nd, ^{178}Hf, ^{182}W, ^{205}Tl, ^{209}Bi

Table 6: Laser settings used for LA-ICP-MS.

	Preablation	**Measurement**
total pattern size	2x1 mm	2x1 mm
pattern design	10 line horizontal “snake pattern”	10 horizontal lines
laser energy	50 % (0.6 mJ)	100 % (1.2 mJ)
laser repetition rate	20 Hz	20 Hz
Laser spot size	100 µm	100 µm
Scan speed	200 µm/s	50 µm/s

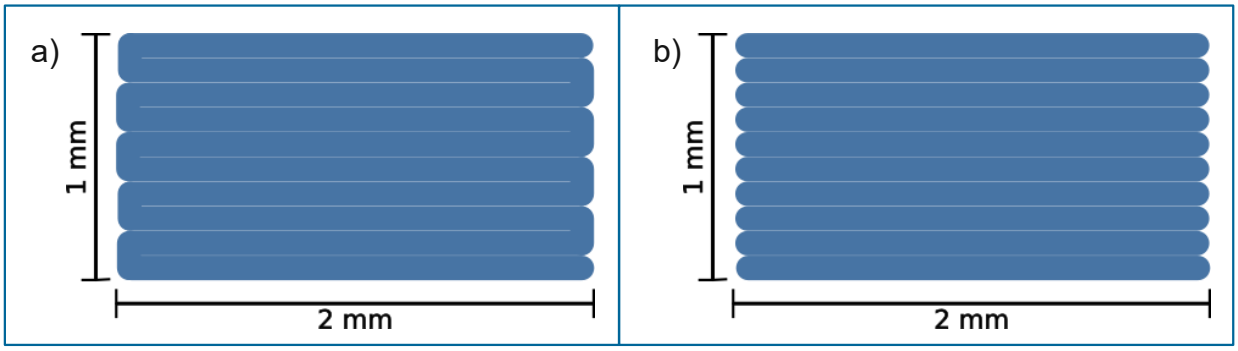

Figure 16: Laser ablation pattern for LA-ICP-MS measurement. a: preablation pattern; b: measurement pattern.

3.6 LIBS measurement

For LIBS measurement, the sample slides prepared for the LA-ICP-MS measurement were placed in the sample chamber of the instrument (J200 Tandem, Applied Spectra) and measured using the integrated 266 nm Nd:YAG laser. The measurement conditions are listed in Table 7 and the ablation pattern is illustrated in Figure 17. The 50 spectra measured on each sample position were accumulated, resulting in 50 datapoints per sample fur further data evaluation. No preablation was performed for these measurements.

Table 7: Measurement conditions for LIBS measurement.

Chamber gas flow	Ar, 1 l/min
Total pattern size	2x1 mm
Pattern design	10 x 5 individual spots, 50 shots per spot
Laser energy	100 % (ca. 3.2 mJ)
Laser beam diameter	100 µm
Laser repetition rate	10 Hz
Laser warmup shots	None
broadband detector:	190 – 1047 nm
Gate delay	0.3 µsec
Gate width	1.05 msec

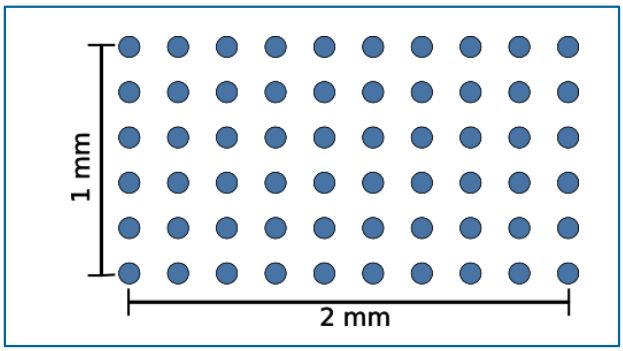

Figure 17: Ablation Pattern for LIBS Measurement.

3.7 Tandem measurement

For simultaneous LIBS and LA-ICP-MS measurement, the sample chamber of the LIBS instrument was connected to the sample inlet of the ICP-MS instrument using Tygon® tubing with an internal diameter of 3.2 mm. The instrument settings for the LIBS and the ICP-MS instruments are listed in Table 8 and Table 9 respectively. Figure 18 illustrates the patterns used for preablation and measurement. 50 parallel line scans with a length of 2 mm and a spacing of 50 µm at a beam diameter of 100 µm were ablated per sample. LIBS data of each line scan (50 shots per line) was accumulated, and ICP-MS data of one line scan was averaged resulting in one LIBS and ICP-MS data point per ablated line. Therefore, again 50 datapoints per sample were obtained.

Table 8: LIBS and laser instrument settings for Tandem measurement.

	Preablation	**Measurement**
Chamber gas flow	He, 0.8 l/min	He, 0.8 l/min
Total pattern size	2x7.35 mm	2x7.35 mm
Pattern design	50 line snake pattern	50 lines, 2 mm length, vertical dist. 150 µm
Laser energy	50 %	80 % (2.7 mJ)
Laser beam diameter	100 µm	100 µm
Laser repetition rate	10 Hz	10 Hz
Laser warmup shots	0	45
Gate delay broadband detector	-	0.3 µsec

Table 9: ICP-MS instrument settings for Tandem measurement.

Plasma Power	1550 W
Dwell time/isotope	10 ms
Ar make-up flow	0.8 l/min
Coolgas flow	14 l/min
Auxillary gas flow	0.8 l/min
Measured isotopes	^{55}Mn, ^{56}Fe, ^{59}Co, ^{60}Ni, ^{121}Sb, ^{138}Ba, ^{140}Ce, ^{141}Pr, ^{146}Nd, ^{178}Hf, ^{182}W, ^{208}Pb, ^{209}Bi

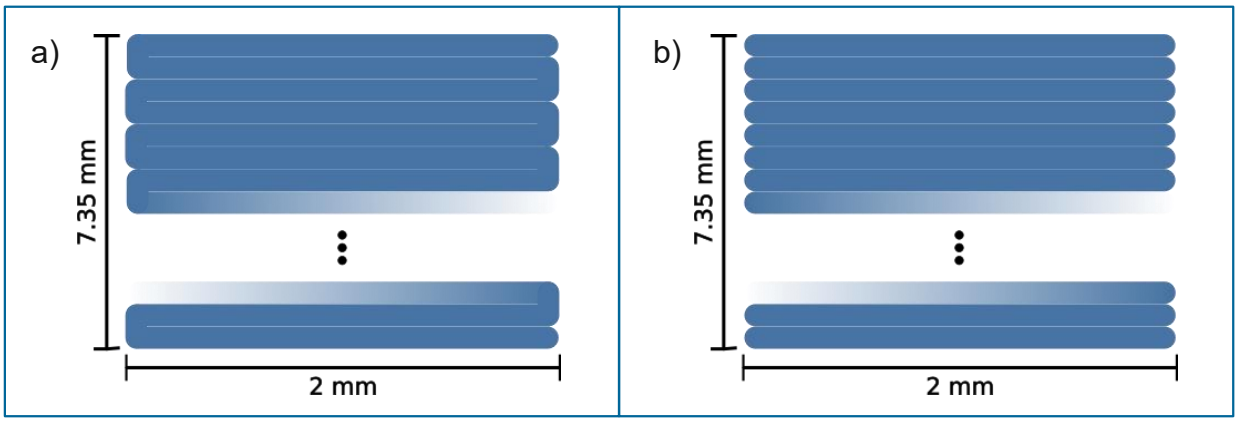

Figure 18: Laser ablation pattern for Tandem measurement. a: preablation pattern; b: measurement pattern. (The spacing between lines is not correctly depicted)

3.8 SEM Imaging

Samples for SEM Imaging were embedded in Epoxy resin and polished using a Struers Tegramin-30 preparation system, using a slurry of 1 µm diamond particles in the last step. To achieve a sufficient electrical conductivity, the sample surface was coated with a thin layer of gold using an AGAR sputter coater (12 mA, 0.08 mbar, 40 sec) before imaging on the electron microscope (Quanta 200, FEI) was performed.

SEM images of sample A1 in three different magnifications are shown in Figure 19.

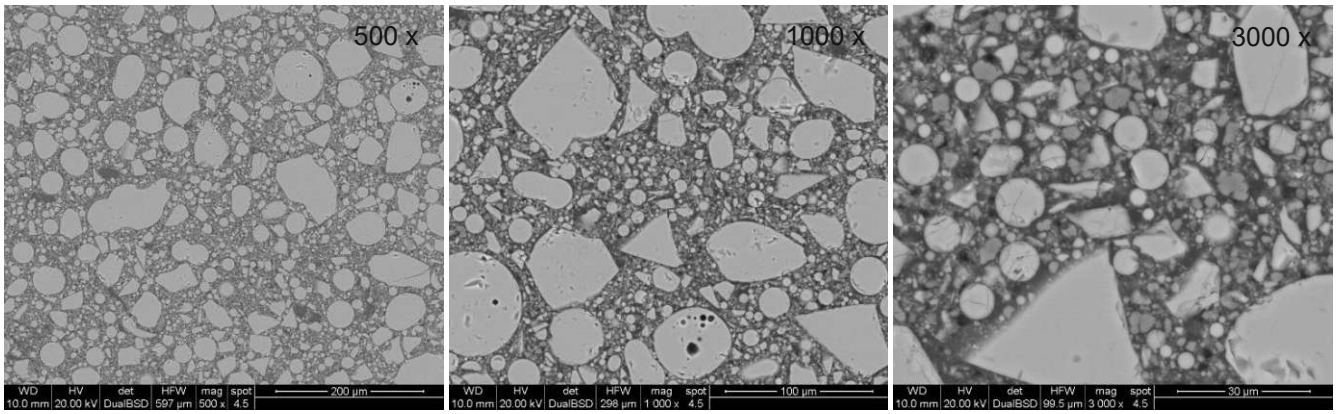

Figure 19: SEM images of one mold compound sample in three magnifications.

EDX-spectra collected (EDAX X1, AMTEK) did not result in a gain in information and are not discussed.

3.9 Dataprocessing and Chemometrics

Initial data preprocessing was performed using ImageLab® (Version 4.20, Epina GmbH, Retz, Austria). Two datasets were created for chemometric evaluation. The first dataset contains the measurement results of the separate LIBS and LA-ICP-MS measurements. The second dataset contains the data from the Tandem analysis. The processing for both datasets was identical.

LIBS spectra were imported into ImageLab and grouped to form a hyperspectral image. The reflection of the laser at 266 nm was cut from each spectrum and replaced by a linear interpolation of the neighbouring points. The spectra were then scaled individually to a mean of 0 and a standard deviation of 1.

ICP-MS data was imported into ImageLab and combined with the LIBS dataset to form a dataset where each pixel in the hyperspectral image possesses a LIBS-spectrum and detected ion intensities.

3.9.1 Selection of spectral descriptors

The measured ion intensities were directly used as descriptors for the ICP-MS spectra. To facilitate the comparison of both datasets, a compromise spectral descriptor set containing only ion intensities that are common to both datasets was generated (^{55}Mn, ^{56}Fe, ^{59}Co, ^{60}Ni, ^{121}Sb, ^{140}Ce, ^{141}Pr, ^{146}Nd, ^{178}Hf, ^{182}W, ^{209}Bi).

For the LIBS-spectra, descriptors were obtained by integration of hand selected emission lines from all samples. The baseline of each emission line was approximated by a straight line.

To make optimal use of the Tandem data, some calculations were also performed on MS data scaled to $^{36}Ar^{1}H^{+}$as internal standard. Spectral descriptor values were exported and used for further data evaluation.

3.9.2 Chemometric analysis

3.9.2.1 Principal component analysis

Principal component analysis was performed using both datasets and all spectral descriptor sets. For principal component analysis, the individual spectral features were standardised to prevent the most intensive emission lines from dominating.

The final PCA plots were generated using Python3 packages pandas[64], scikit-learn[65] and matplotlib[66] and the library adjustText[67].

3.9.2.2 Hierarchical cluster analysis

Hierarchical cluster analysis was performed on the optimised Tandem dataset with LIBS descriptors (b) and all available ion intensities using DataLab® (Version 4.980, Epina GmbH, Retz, Austria).

3.9.2.3 Random decision forest

Random decision forest classifiers were calculated using Python3 packages pandas[64] and scikit-learn[65].

4 Results and Discussion

4.1 ICP-MS measurements of digested samples

Analysis of the diluted sample digests delivered signals above the detection limits for most elements. To obtain quantitative data, the calibration functions shown in section 3.4 were used to determine the elemental concentrations in the diluted solutions of sample digestions and digestion blanks. Using the dilution factor that was determined gravimetrically for each measured sample, the elemental concentrations in the undiluted digestion solutions was determined. The digestion blanks were used to correct the concentration determined in the sample solutions for any background caused by the utilised acids and instruments. From the concentrations in the digestion solution and the known weight of the mold compound sample utilised in each digestion, the elemental concentrations in the solid mold compound sample were calculated. The results are displayed in Figure 20. The bar diagrams show the mean elemental concentration in the solid molding compound samples. The error bars show the standard deviation calculated from 15 total measurements performed of each sample (5 instrument replicates of each of the three digestions performed per sample).

The following isotopes were successfully used for quantification: 7Li, 9Be, 24Mg, 27Al, 52Cr, 55Mn, 57Fe, 58Ni, 59Co, 65Cu, 66Zn, 71Ga, 88Sr, 121Sb, 140Ce, 141Pr, 143Nd, 178Hf, 184W, 203Tl, 209Bi

Quantification of 23Na, 39K, 44Ca, 112Cd, 120Sn, 125Te, 137Ba, 139La and 208Pb was attempted but unsuccessful due to:

- high background signal caused by contaminants in the reagents and instrument itself
- loss of analytes due to the formation of insoluble or gaseous compounds during digestion
- spectral interferences.

The digestion results show many differences in sample composition. Only two of the ten investigated molding compounds, B1 and B2, contain significant amounts of both Boron and Zinc, pointing to the use of Zinc borate as flame retardant[68]. Zinc, but not boron is also included in mold compound C1, where a different zinc compound seems to be in use. Aluminium, which is also used as a flame retardant in polymers in the form of Aluminium Trihydrate [69] on the other hand was detected in all samples, although the concentration varies with the type of molding compound. Magnesium was detected in varying amounts in all of the Molding compounds, with the exception of B1 and B3, the two boron containing types. It can be assumed that its purpose is flame retardation as well, possibly in the form of Magnesium Hydroxide[70]. Bismuth, only detected in molding compound A3, is also used as a flame retardant in the form of Bismuth oxide[71].

Concentrations of minor constituents also vary between molding compound types. Some elements only appear in a single investigated type, such as bismuth and hafnium, while others are contained in multiple molding compounds, such as iron, tungsten, gallium, cerium, praseodymium, beryllium and thallium. Some elements could be found in all of the investigated sample, but in varying concentrations, such as lithium, nickel, copper and strontium.

While the elements detected in high concentrations (10^4 ng/g and above) were most likely added to the material on purpose, those constituents detected in very small quantities can also constitute contaminants originating from the raw materials or the manufacturing tools used to process the molding compound. These elements might not be representative for the material as a whole but only for the specific batch and manufacturing conditions used for the preparation of the investigated sample tiles.

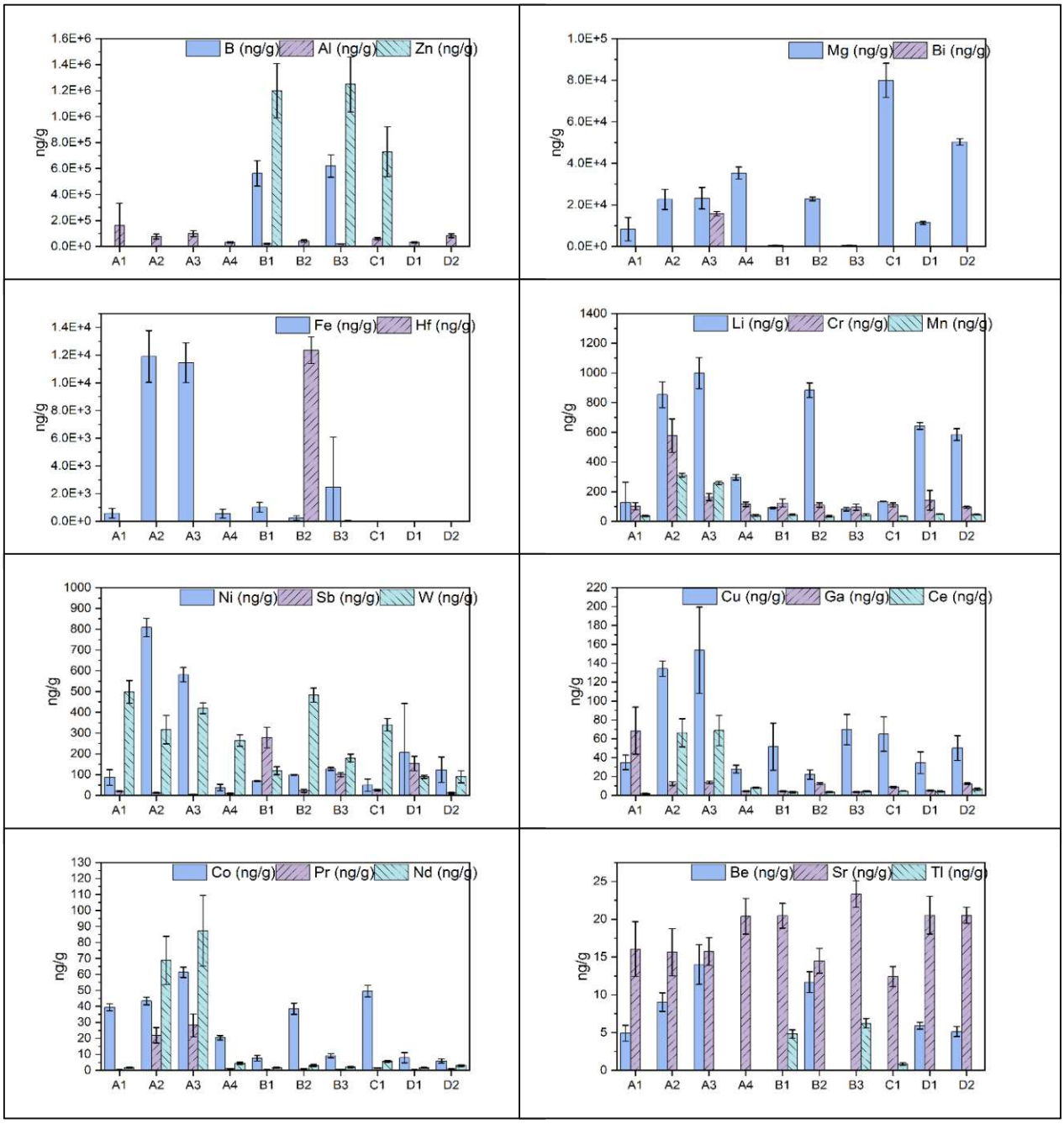

Figure 20: Results of ICP-MS measurements of digested samples.

Although there is a good reproducibility of the measurements for most samples and elements, the absolute elemental concentrations are not reliable for several reasons.

- Misalignment of the IR- temperature probe of the microwave digestion system led to higher digestion temperatures than planned, causing excessive venting and probable loss of more volatile elements and compounds.
- The addition of HF, made necessary by the high content of SiO_2 leads to the formation of insoluble fluoride compounds, reported in literature for Al, Ca, Mg, and Fe[72] as well as Na[73].
- The high number of digestions made it necessary to store some digestion solutions for several days prior to dilution and measurement, leaving ample time for ion adsorption to the walls of the centrifuge tubes and depletion of the solutions.

- Storage of the digestions in centrifuge tubes for several days also provided ample time for contaminants in the PE vessel walls to be leached into the sample solution.

As all samples underwent the same preparation process and were therefore subject to the same influences, the qualitative comparison of results of different molding compounds is still valid and can be used as starting point for a selection of elements for detection with LA-ICP-MS. As the liquid ICP-MS measurements were only intended as a starting point for subsequent laser ablation experiments, the method was not further optimised to obtain true quantitative results.

Some samples are very distinct in their elemental fingerprint, especially those that contain an element that is unique to them, such as bismuth to molding compound A3 and hafnium to B2, while others show more similarity. The most notable similarity can be observed between molding compounds B1 and B3. Not only are these the only samples containing boron, the concentration of all other investigated elements is nearly identical as well, with the exception of a higher antimony concentration in B1. Samples D1 and D2 are very similar as well, although they differ in their magnesium content as well as their antimony content.

4.2 Exploratory data analysis

In a first step the obtained data is investigated using exploratory data analysis. Principal component analysis and hierarchical cluster analysis is employed to get an understanding of the structures present in the data and to find relationships between samples. The exploratory data analysis was also used to assess if the dataset might be used to build a classifier, and to find the most promising combination of measured data and spectral descriptors for the building of a classifier. Therefore, all available datasets were investigated. Three distinct sets of data were obtained by the measurements described in the methods section: LIBS measurements, LA-ICP-MS measurements, and the Tandem measurements, consisting of LIBS and ICP-MS data.

4.2.1 LIBS data

The first data set recorded and investigated was the separately measured LIBS data. Figure 21 shows the exemplary LIBS spectra of 4 different molding compound samples. These spectra were generated by accumulating 50 single shot spectra originating from the same lateral sample location during measurement. As was to be expected, intense emission bands of Si are present in all measured spectra. Other elemental emission lines like C, H, O, Li, Na, Mg, K, Ca, B, Mo, Al, Zn, and Zr could be identified in varying intensities in multiple or all the samples. An emission line for Sb could be detected in sample C2 only, which was not included in the sample set for ICP-MS after microwave digestion. The Intensities of the Zn, B, Al, Li and Mg lines were consistent with the ICP-MS results obtained before, with Zn being also present in C3 and C4, and A6 containing little to no Mg as well. The emission line of C_2-band was very weak in all spectra.

In addition to the emission lines of the elements contained in the sample and argon used as chamber gas, all spectra contain a very intensive reflection of the laser light at 266 nm, that is removed from the spectra before further processing steps.

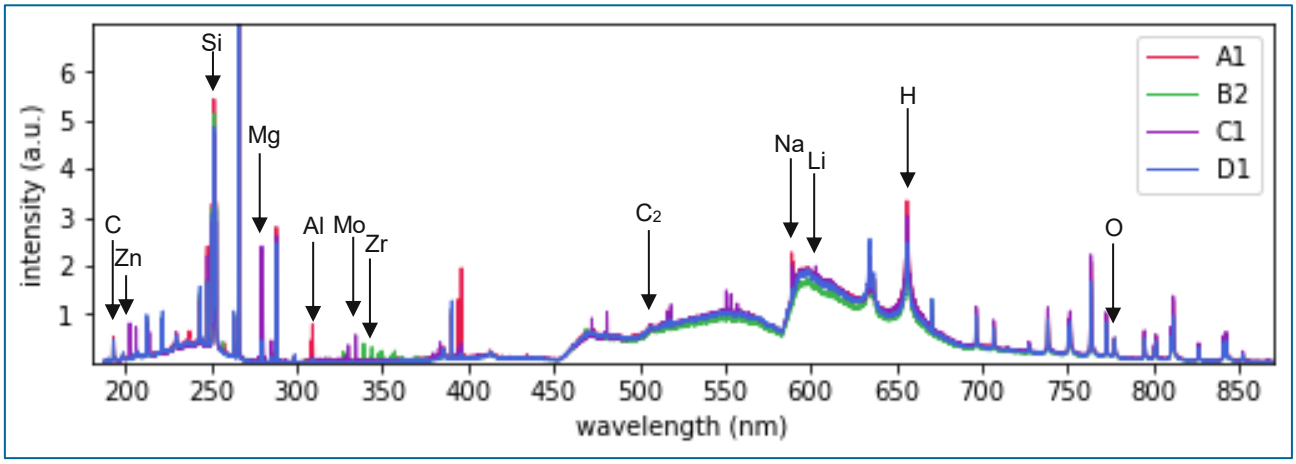

Figure 21: LIBS broadband spectra of molding compounds A1, B2, C1 and D1.

For the subsequent data analysis, reproducibility is important. To correct for variation in laser intensity, each spectrum is scaled to a standard deviation of 1 and transposed to a mean of 0. The variation in intensity between the 50 spots measured per sample reveals information about the reproducibility of the measurements as well as sample homogeneity. If the sample is homogeneous and the measurement reproducible, the variation between spots is low. A high variation can point to either inhomogeneity in the sample, especially if only some elements are affected, or a low reproducibility in instrumental measurements.

The relative standard deviation of a signal is only a meaningful figure if the signal is significantly higher as the background noise of the detector. Depending on signal intensity of major and minor constituents, the relative standard deviation of signals varies between 4 and 20 percent in those cases.

4.2.1.1 Influence of LIBS spectral descriptor selection on PCA

For chemometric analysis, the dimensionality of the LIBS spectra was reduced using the approach of spectral descriptors described in 2.7.2.2 . The emission lines to be used as spectral descriptors were selected by hand and different sets of descriptors were examined by looking at the resulting PCA plots.

The first descriptor set (a) includes all emission lines visible in any spectrum, except for emission lines that could be identified as originating from the Ar gas in the ablation chamber and contains 109 descriptors.

The PCA-plots of this descriptor set (Figure 22) show the Zr-lines to dominate the first two principal components, allowing for the distinction of molding compound type B2. Additional principal components show a separation of molding compound type A1, A8 and C2 from all other sample points in different projections. Types B1 and B3 are mapped closely together in all inspected projections, but are removed from other samples in some projections. Samples C1, C2 and C4 form their own separate cluster in the PC1/PC3 and PC3/PC4 plot.

Descriptor set a): all LIBS Lines

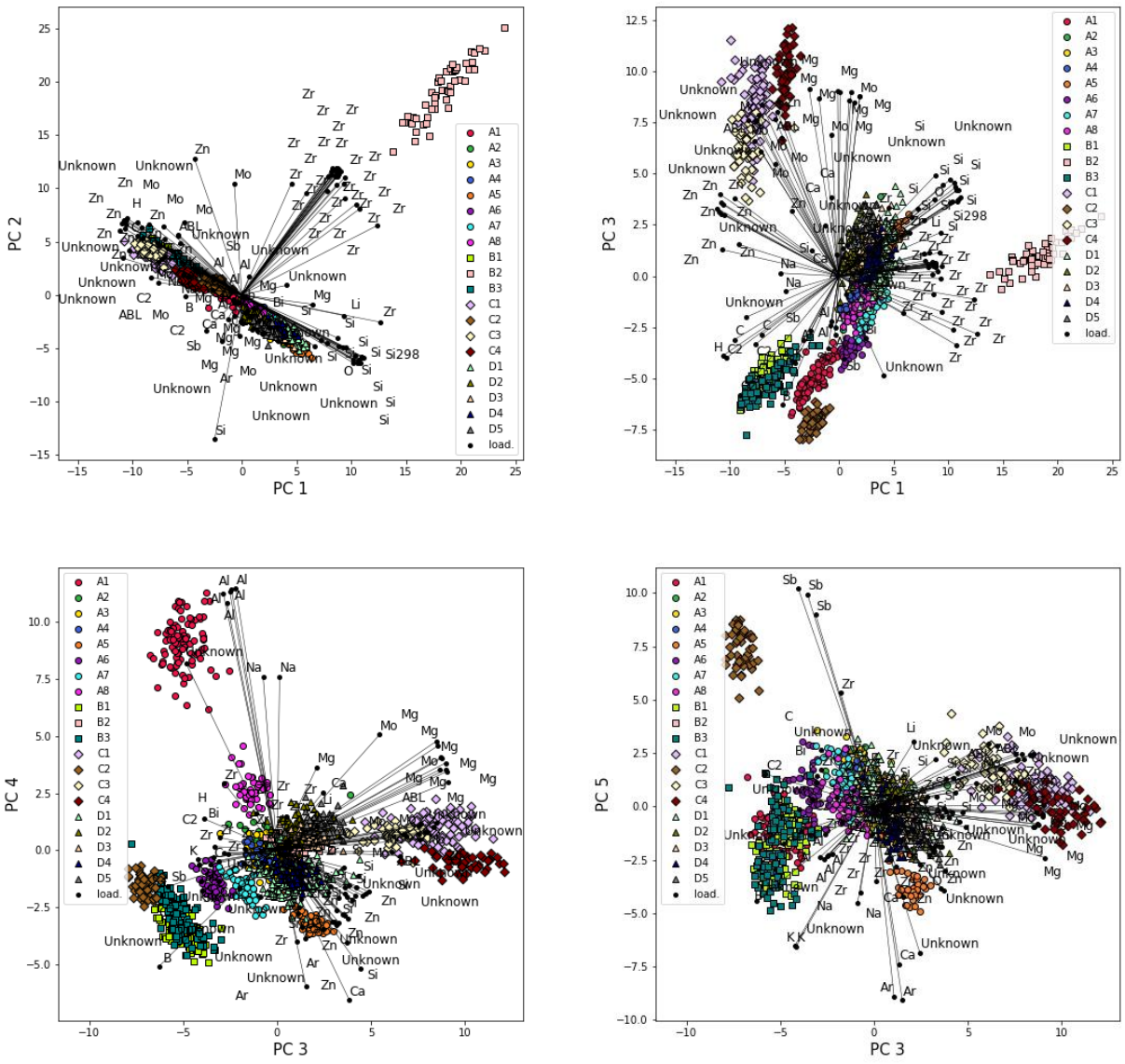

Figure 22: Selected bi-plots of the PCA using descriptor set (a)

To further reduce dimensionality and to remove the emission lines of unknown origin, a second descriptor set was constructed. This descriptor set (b) only contains emission lines of identifiable origin, with a maximum number of 10 lines per element. This reduces the number of spectral descriptors from 109 to 71.

Without the dominating Zr-Lines, the descriptor set (b) shows a greater differentiation between molding compound types in the early principal components. All molding compound types that separate from the bulk in set (a) continue to do so. The separation between types C1, C3 and C4 is better visible, as well as the separation between A6 and A7.

In the PC2/PC5 projection, type B1 splits into two clusters, most likely due to different sample types (package, tile) of the two measured samples of this type. The same can be observed with type B3.

Descriptor set b): number of Zr-Lines reduced; unknown lines removed

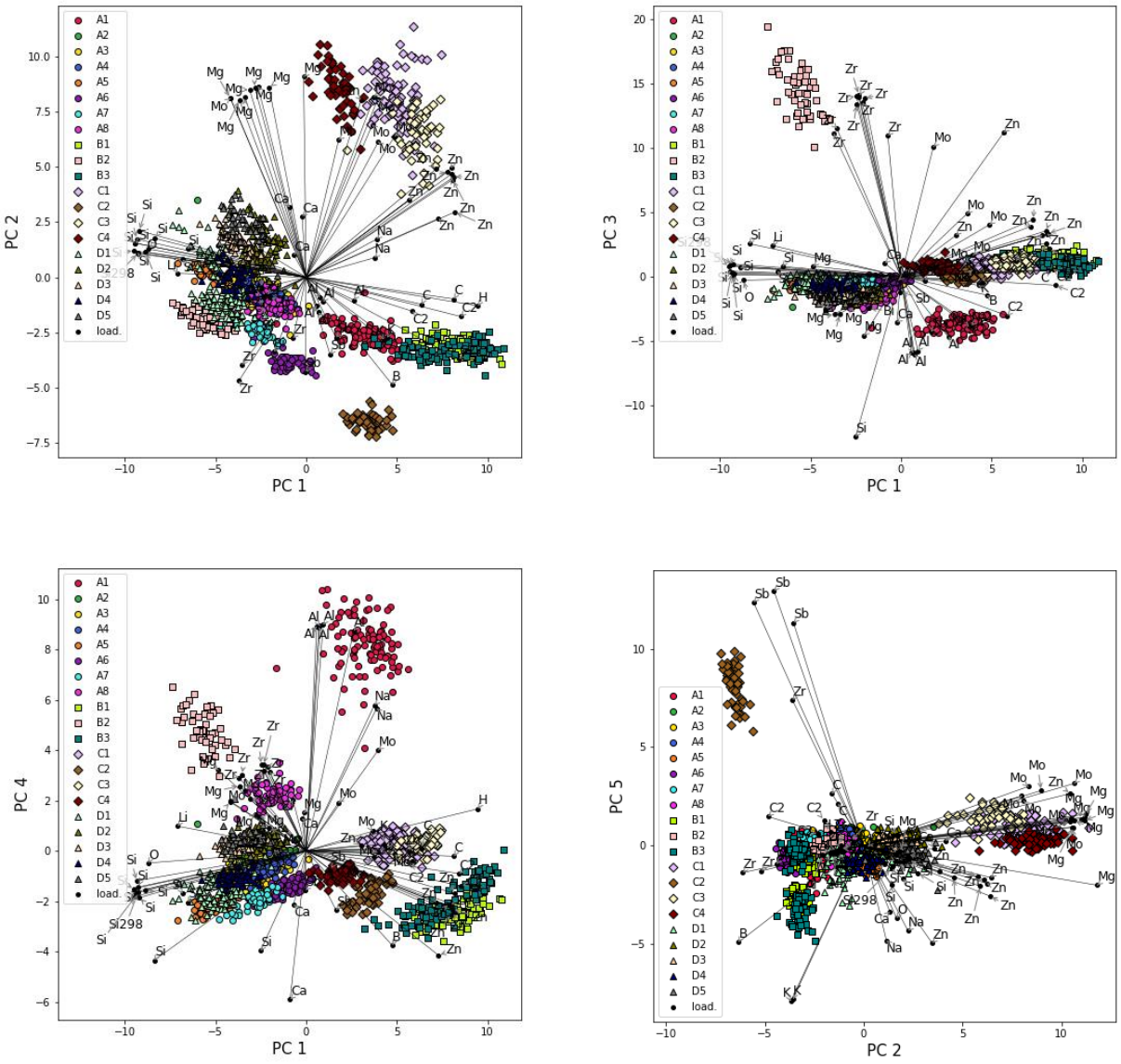

Figure 23: Selected bi-plots of the PCA using descriptor set (b)

To get the cleanest, most easily interpretable PCA plots possible, the descriptor set was reduced further, to only contain a maximum of 2 line per element. The resulting descriptor set (c) only contains 20 descriptors. The PCA using the smallest descriptor set (c) shows the same principal pattern of samples clustering together, as demonstrated in Figure 24.

Here, the measurements of samples A1, B1 and B3 separate into two clusters. As these are the only molding compound types where both tile shaped and finished package samples were measured, it is safe to assume that the split of the clusters is caused by the difference in sample type. Possible explanations for the differences in chemistry are oxidation of the surface and chemical changes caused by the zinc-coating process for the leads. As all descriptors comprising descriptor set (c) are also included in sets (a) and (b), this split is also present in the previous PCAs even though it is not visible in the projections of the first principal components, which is shown here.

Descriptor set c): 1-2 LIBS emission lines per element or molecule

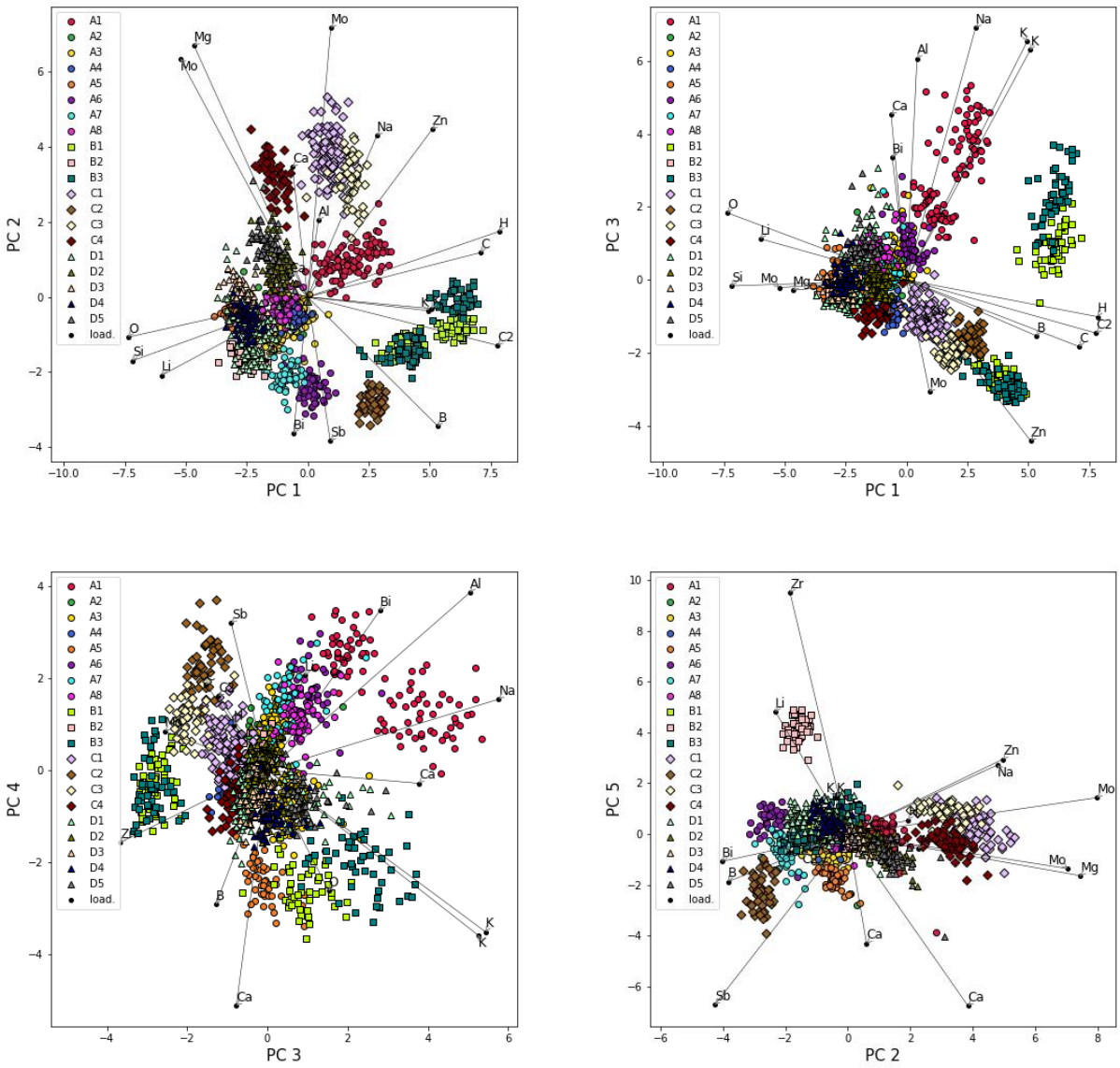

Figure 24: Selected bi-plots of the PCA using descriptor set (c)

While this reduced dataset results in the most easily comprehensible PCA-plots and reveals the splitting of some samples, relevant information for the classification could be lost. Of the three descriptor sets discussed, the second one (b) was identified as the most promising for further analysis by inspection of the clustering behaviour in the PCA plots.

4.2.2 LA-ICP-MS data

The selection of elements for LA-ICP-MS was based on the results of the liquid ICP-MS measurements. A smaller set of elements had to be selected, to ensure that the sequential measurement of the quadrupole ICP-MS collected a sufficient amount of data points for each element during laser ablation. Due to this restricted number of analytes, elements not accessible to LIBS due to their low concentration in the material were favoured for MS analysis. The isotopes ^{10}B, ^{25}Mg, ^{34}S, ^{53}Cr, ^{55}Mn, ^{56}Fe, ^{59}Co, ^{60}Ni, ^{63}Cu, ^{71}Ga, ^{121}Sb, ^{140}Ce, ^{141}Pr, ^{146}Nd, ^{178}Hf, ^{182}W, ^{205}Tl and ^{209}Bi were originally measured, but only ^{55}Mn, ^{56}Fe, ^{59}Co, ^{60}Ni, ^{121}Sb, ^{140}Ce, ^{141}Pr, ^{146}Nd, ^{178}Hf, ^{182}W and ^{209}Bi were used for data analysis, as they contributed additional information to the LIBS data and did not suffer too much from interferences.

The following Figure 25**Fehler! Verweisquelle konnte nicht gefunden werden.** shows the first 100 seconds of transient ion intensity signal detected during the LA-ICP-MS measurement of samples B2 and D1. The signals originating from the individual lines of the ablation pattern are clearly distiguishable due to the drop in intensity in between. The signal intensity over time is relatively stable for higher intensities, with bigger variations in ion signals at lower intensity. The variations observed are caused by the changes in gas flow rates etc. in the measurement system. Some superimposed spikes might be caused by inhomogeneities in the sample, but due to the fluctuations in signal intensity, they can not confidently be identified. A comparison of the measurement results of different samples shows qualitative differences bertween molding compounds.

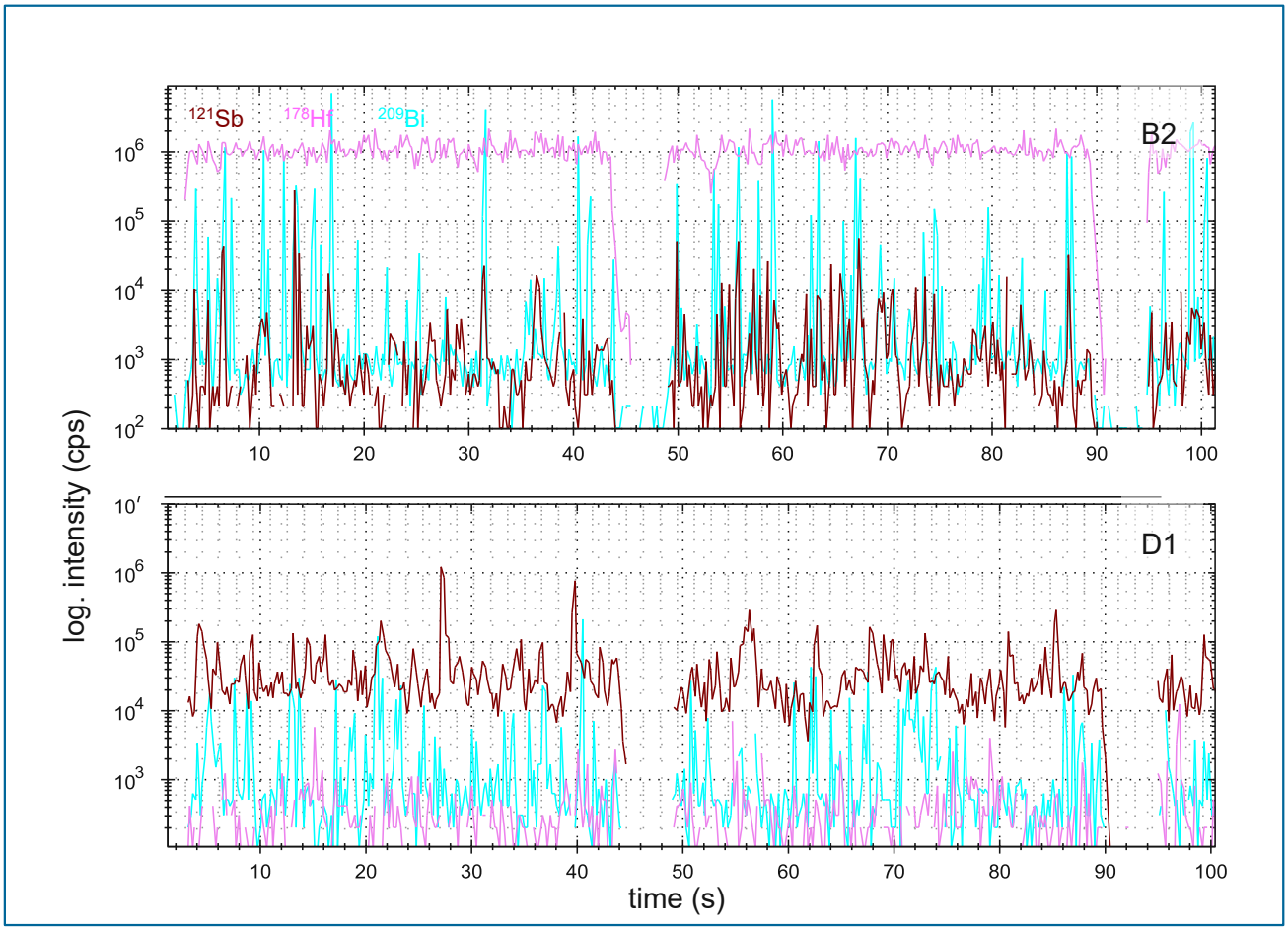

Figure 25: Transient ion signal of ^{121}Sb, ^{178}Hf and ^{209}Bi recorded during the first 100 seconds of LA-ICP-MS measurements of samples B2 and D1.

To obtain 50 data points per measurement, the transient signal of each of the 10 lines of the laser ablation pattern was divided into 5 sections of equal length for evaluation.

The data from the LA-ICP-MS measurement was evaluated on its own and in combination with the LIBS dataset discussed above. For the LA-ICP-MS data, the 11 measured ion intensities listed above were directly used as spectral descriptors.

Using only MS-descriptors, the samples form 4-5 clusters in the first 3 principal components (A2+A3+A4+A8, A6, A7, B1+B3+C2, and all other types). Compared to the bi-plots obtained from LIBS, there is an increased amount of spreading of the measurements.

The combination of the separately measured MS and LIBS descriptor sets results in Bi-plots that are very similar to the LIBS-only results which is not surprising given that the number of spectral descriptors generated from LIBS data is much higher compared to LA-ICP-MS. The LA-ICP-MS data does not seem to significantly improve the quality of the data set for the purpose of differentiating between different types of mold compound.

Comparison of PCA-bibi-plots: top row: LIBS descriptor set (b); middle row: LIBS descriptor set (b) and MS descriptors; bottom row: only MS-descriptors

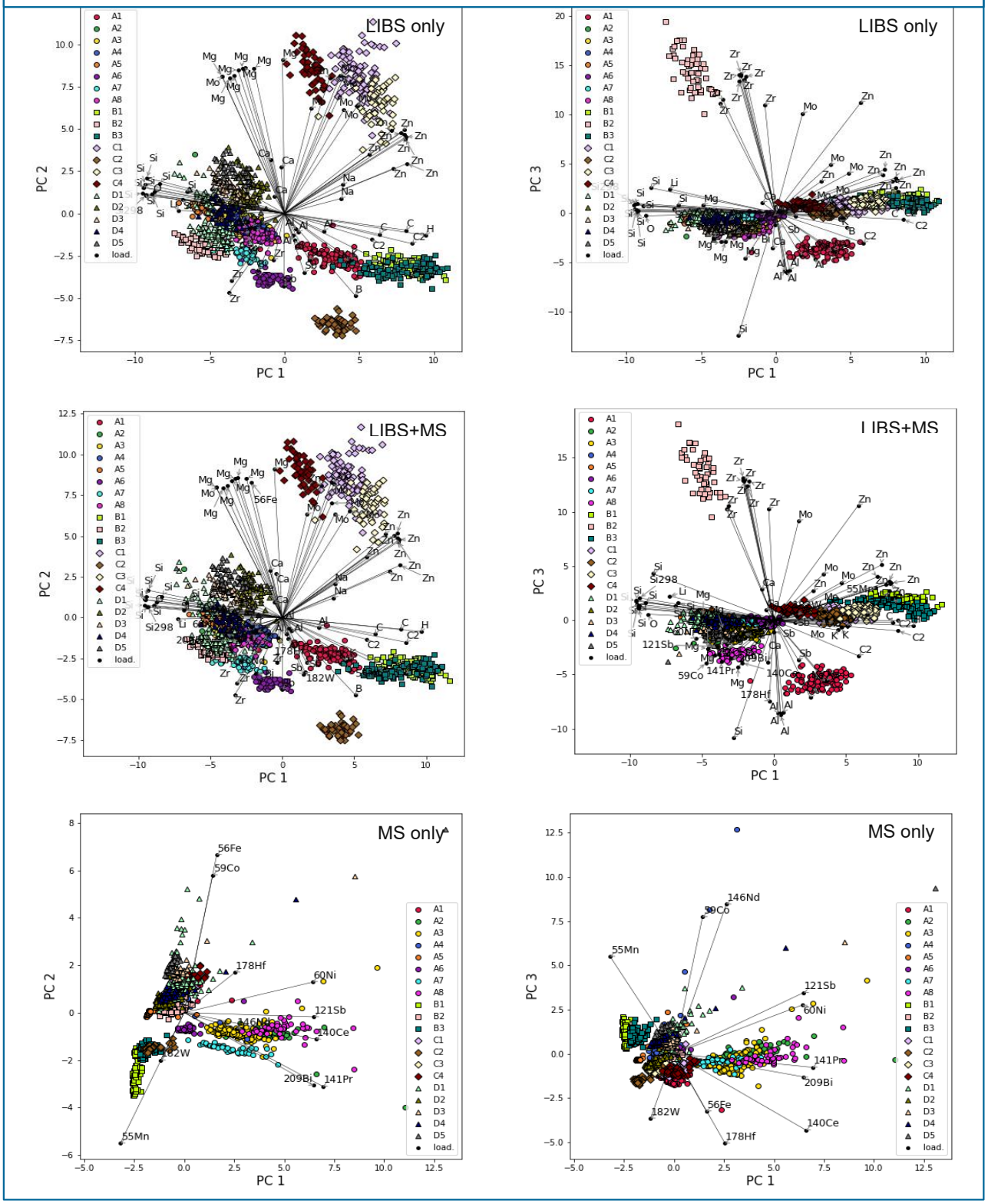

Figure 26: PCA Plots of LIBS and LA-ICP-MS datasets: LIBS data only (upper row), both LIBS and MS data (middle row), MS data only (lower row).

4.2.3 Tandem measurements

As the tandem dataset was measured after the first LA-ICP-MS dataset, some changes based on knowledge gained in the meantime were made to the selection of ions to be measured, including the measurement of ArH^+ at m/z 37 as internal standard to compensate for changes in the MS detection system.

The ion intensities of the tandem measurement using a 266 nm laser are approximately one order of magnitude lower than the ion intensities of the LA-ICP-MS measurement performed with the 213 nm laser. A comparison of the signal stability is difficult, due to the different duration of the laser ablation. While the previous LA-ICP-MS experiment had continuous signal for 45 seconds at a time, the ion signal of a single line of the ablation pattern of the tandem measurement was detected in 9 seconds, leaving not enough time to reach a stable intensity plateau, as can be seen in Figure 27.

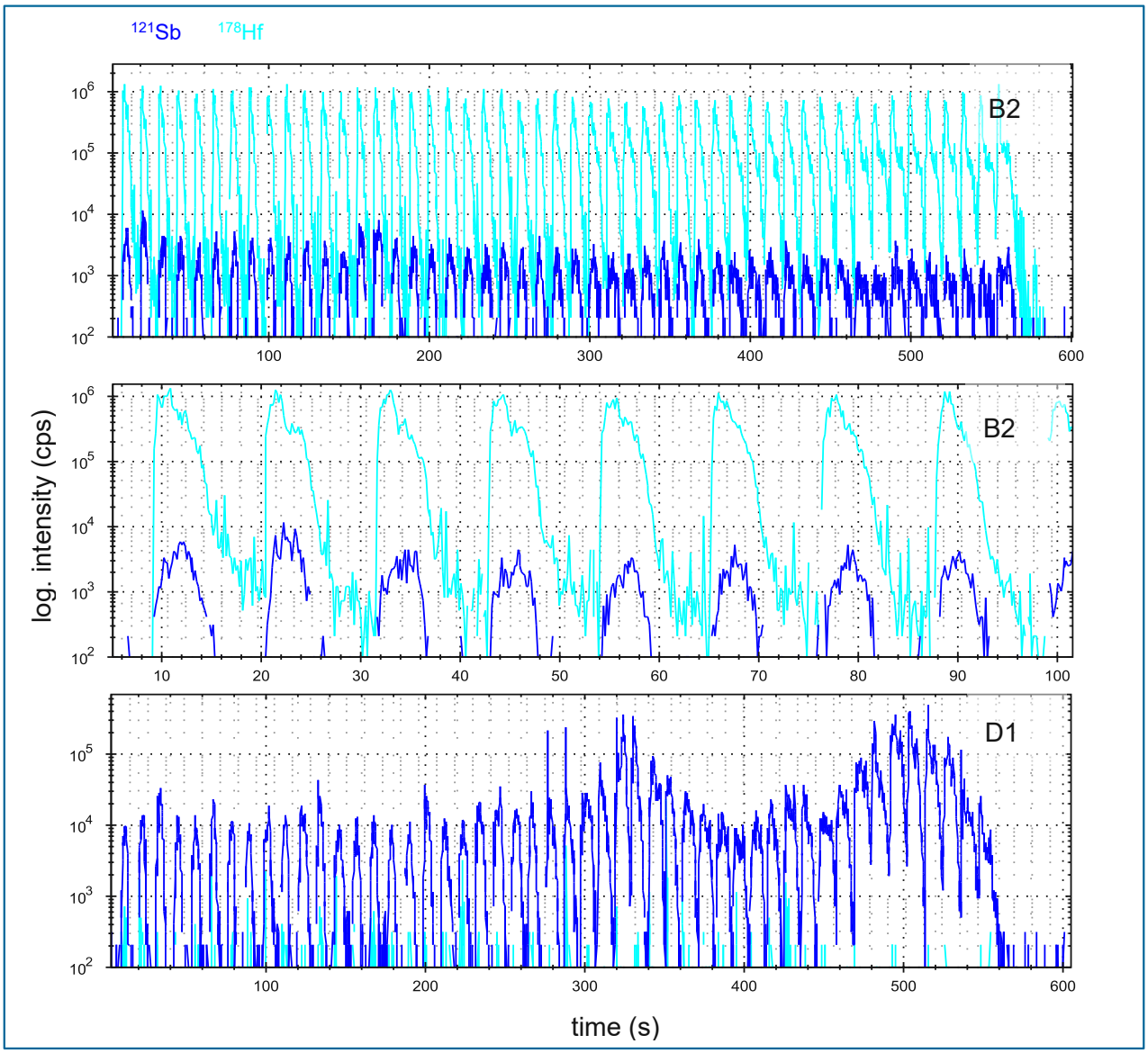

Figure 27: Ion intensities of the Tandem measurement of molding compounds B2 and D1.

The fact that a line of the Tandem pattern consists of only 15 laser shots also impacts the quality of the LIBS spectra. The weakest emission lines from the LIBS measurement are no longer detectable. The relative standard deviation of more intensive lines is similar to the separate LIBS measurement at 4 – 20 %.

To compare the quality of data gained by Tandem measurement to the first dataset using PCA, the same descriptor sets as before were used and no internal standard correction was performed. In a second step, the influence of internal standard correction and use of all available ICP-MS data on the PCA was observed.

4.2.3.1 Comparison to first data set using previous descriptor sets

Figure 28 shows a comparison of PCA plots from the first, separately dataset and the Tandem dataset, using the same pre-processing procedures and descriptor sets.

Comparison of Tandem data (top row) to separately measured data (bottom row) using LIBS descriptor set (b) and LA-ICP-MS ion intensities common to both data sets

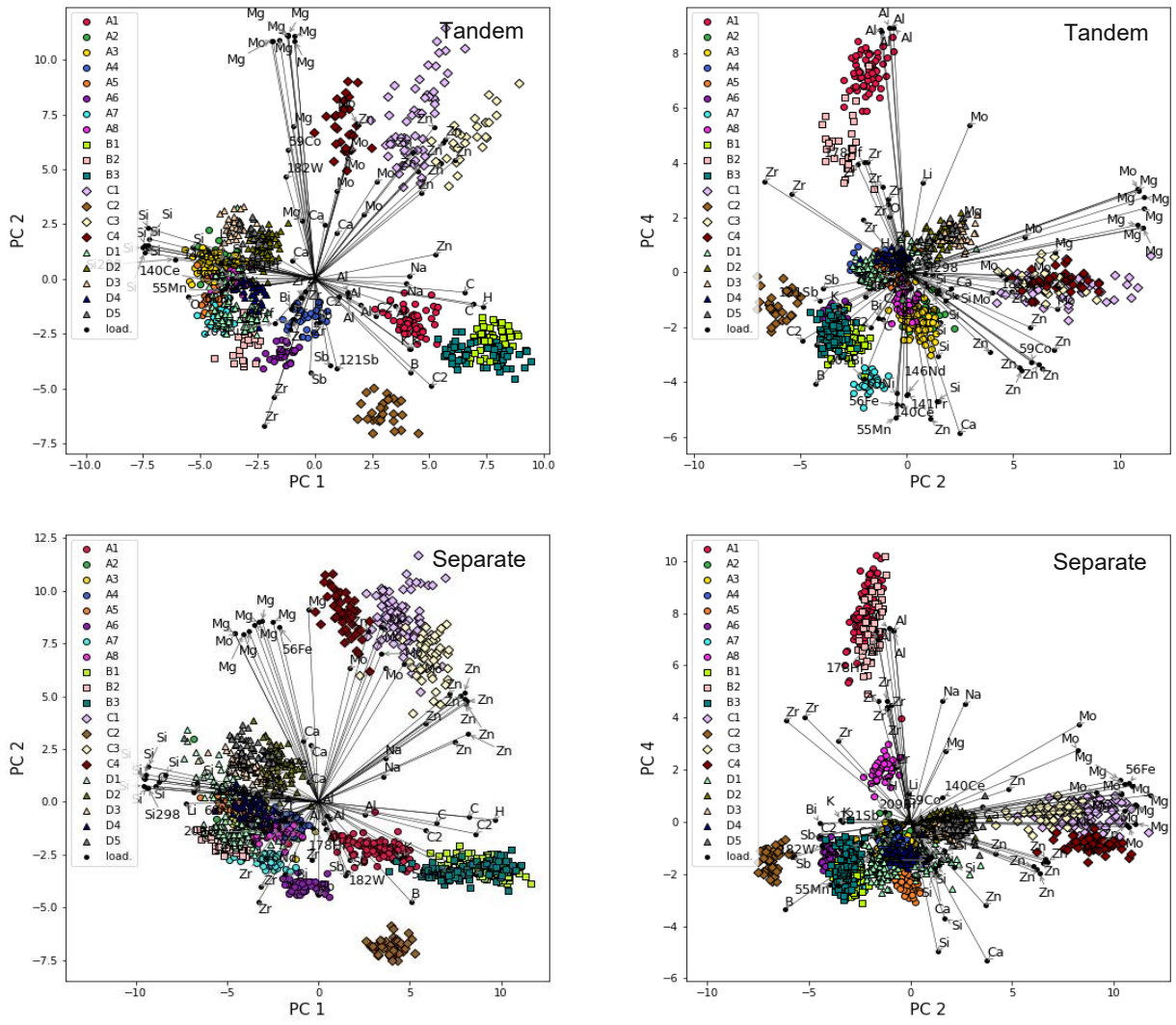

Figure 28: PCA Plots of Tandem (upper row) and separately measured data(bottom row).

4.2.3.2 Complete LA-ICP-MS descriptor set and internal standard corrected data

The plots shown in Figure 29 were constructed using the full potential of the Tandem dataset, making use of the possibility of internal standard correction for the MS signals and all measured ion intensities.

Tandem data: top row: MS data only, all available ion intensities after standard correction; bottom row: MS data in combination with LIBS data, descriptor set (b)

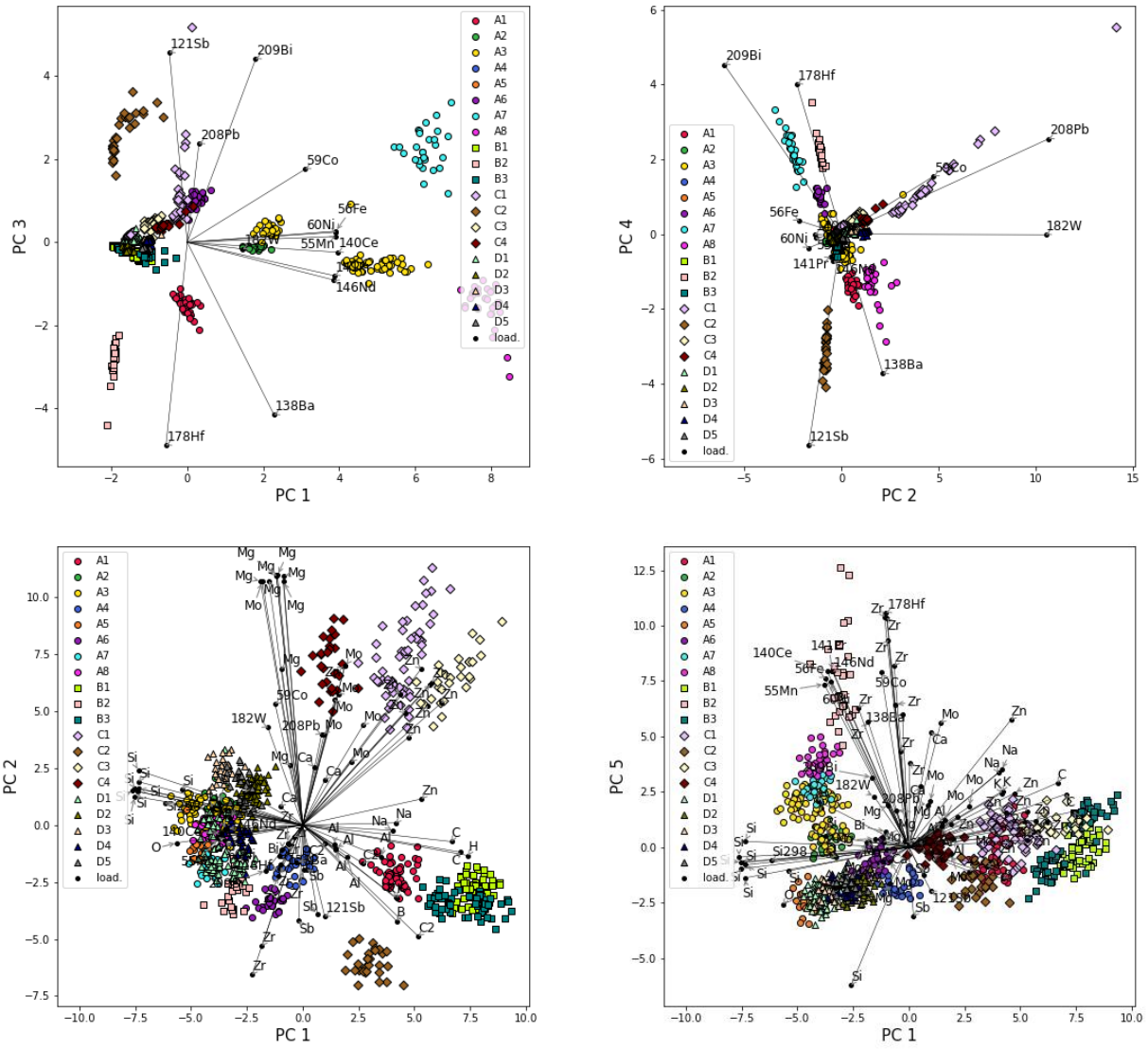

Figure 29: PCA bi-plots of internal standard corrected Tandem data.

Full use of the Tandem dataset shows further improvement in the separation of C1, C3 and C4. The PC1-PC5 bibi-plot shows a separation of the A3 tile and cull samples.

4.2.3.3 PCA and sample manufacturer

To make the different manufacturers of the molding compound samples more visible, the bibi-plot of the Tandem measurement in Figure 30 has been coloured according to manufacturer. All molding compounds of Manufacturer D are located in the left part of the figure. With the exception of type C2, which contains Sb, all molding compounds of Manufacturer C contain Zn or Mo and are located in the upper half of the figure. Two of the three samples of manufacturer B (B1 and B3) were already noted to be very similar.

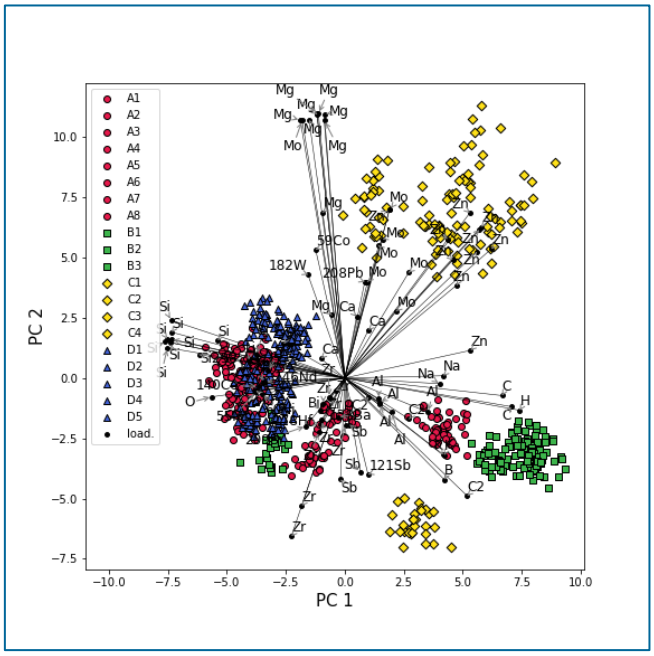

Figure 30: BiBi-plot of Tandem measurement, samples coloured according to manufacturer

4.2.3.4 Hierarchical cluster analysis

Hierarchical cluster analysis was used as an additional tool to visualize similarities between different molding compound types. The dendrogram in Figure 31 shows the result of a hierarchical cluster analysis of the complete tandem dataset, consisting of LIBS and ICP-MS data. The lower section of the dendrogram is magnified in Figure 32.

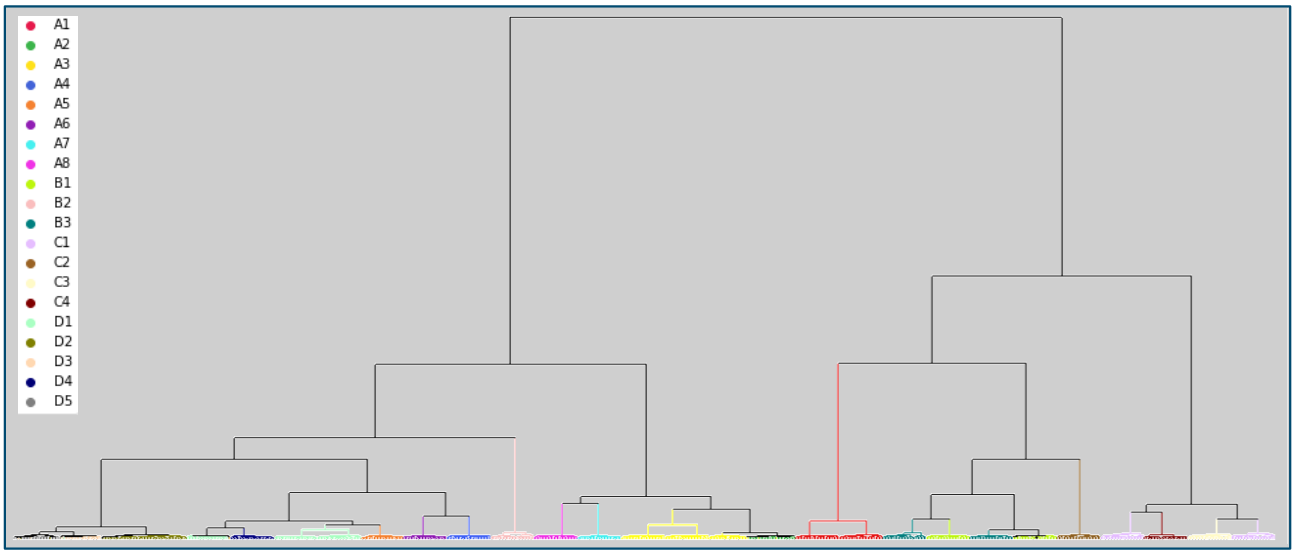

Figure 31: Hierarchical cluster analysis, using Ward's method, Manhattan distance and standardized data of the optimized Tandem measurement (LIBS and all MS lines).

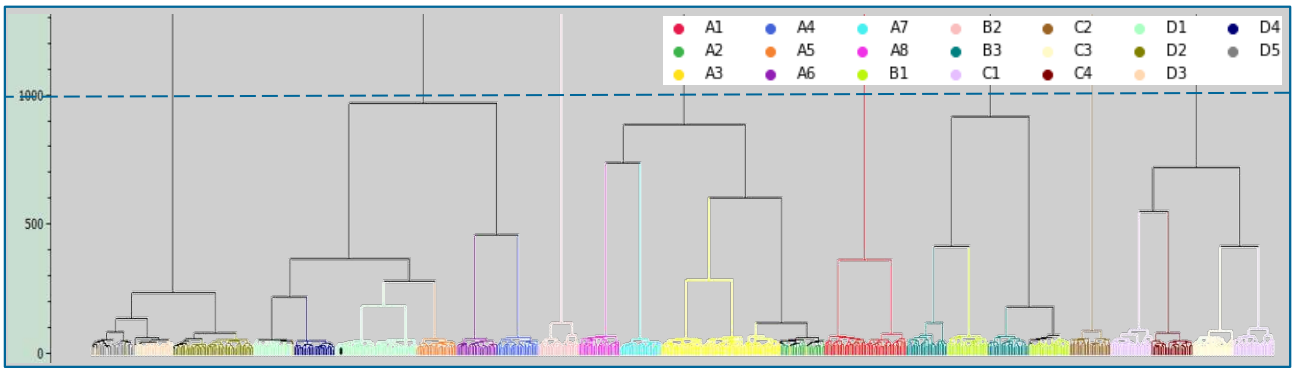

Figure 32: Magnification of the lower section of the hierarchical cluster analysis.

In Figure 32 relatively pure clusters corresponding to the individual samples are observed. Unfortunately, the distance between samples of the same molding compound type is sometimes significantly larger than the distance between samples of different molding compound types. The most extreme examples are types B1 and B3, but A3, C1 and D1 separate as well.

4.2.4 Adaptation of the descriptor sets

The splitting of some sample classes according to sample type (tile, cull or package) in PCA and HCA is detrimental to the training of a classifier. Inspection of the PCA-plots reveals that the split occurs mostly in direction of Li, Na and K LIBS emission lines as well as Ba, W, Pb and Bi ion intensities. It can be assumed that these elements enter the molding compound material during the molding process, originating from the molding tool or the release agent and are therefore present in different quantities depending on the sample type and place of origin. Additionally, Na and K are ubiquitous elements which are often found as contamination independent of the sample type. Therefore, for a classification of sample class independent of the sample type, these elements should be disregarded.

Figure 33 compares the PCA plots of the LIBS data set with the most reduced descriptor set (1-2 Lines per element) with and without the inclusion of Li, Na, and K.

Influence of Na, Li and K: 1-2 LIBS emission lines per element or molecule

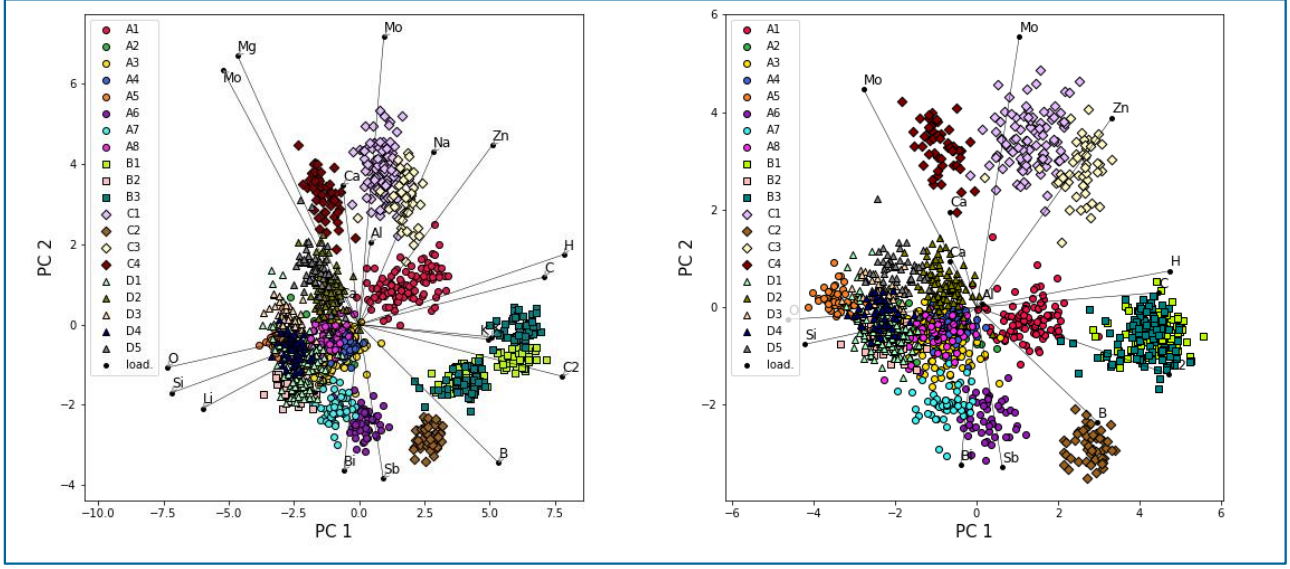

Figure 33: LIBS PCA plot with reduced descriptor set. Left: including Li, Na, K, right: excluding Li, Na, K

The obvious split of B1 and B2 is no longer present after exclusion of Li, Na and K, which is advantageous for the generation of a classifier.

4.3 Random decision Forest

With the information gained by the exploratory data analysis, the following datasets have been chosen for the generation of a classifier:

- The separately measured LIBS data, using a reduced set of 61 descriptors obtained after removing the Li, Na and K emission lines for attribute generation.
- The Tandem data, using the same LIBS descriptors in addition to 9 ion intensities.

To evaluate of the removal of the descriptors had a positive impact on the quality of the classification, two additional classifiers were trained using the descriptor without removing the concerning elements:

- The separately measured LIBS data, using the full descriptor set (b)
- The Tandem data, using the full LIBS descriptor set (b) and all ion intensities.

All steps of model development were performed separately for all four datasets, to enable a comparison of the performance of the final models.

As explained in 2.7.3.2, the available dataset has to be split into a training set and a test set. The most common way to split a dataset is to generate two random subsets of equal distribution, with the test set consisting of 20-25 % of all data points. Because of the splitting of data observed in 4.2.3.4, a different approach was chosen. To make the testing of the model more realistic to a potential later application, all data points measured from a sample were assigned to the test or training dataset collectively. This approach makes sure that the data in the test set is truly independent from the training set, hereby making sure that the model has not simply memorised the individual samples, but differentiates by molding compound types[74].

The samples listed in Table 10 were chosen as the test dataset and excluded from model development. The choice of samples for the test data set was dictated by the availability of multiple samples of the same mold compound type. All remaining samples were used as training dataset for model development and cross-validation.

Table 10: Samples set aside as test dataset.

Test sample	
A1	package
A3	cull
B1	package
B3	package
C1	cull
D1	cull
D2	cull

4.3.1 Hyperparameter optimization

To find the best possible random decision forest model, four hyperparameters were optimised: The number of decision trees constituting the forest, the split criterion used in generating the individual trees, the share of attributes (also called “features”) examined at each split and the share of samples of the training set used to build each tree. For each possible combination of hyperparameter values, a cross validation with 10 repetitions was performed using a 90/10 split.

The following values for the hyperparameters were tested:

- Number of decision trees: 50, 75, 100, 150
- Split criterion: gini, entropy
- Share of attributes (or “features”) considered per split: 0.01, 0.05, 0.1, 0.2, 0.3
- share of total samples considered per tree: 0.2, 0.5, 0.75, 1.0

The following Table 11 lists the hyperparameter combination resulting in the best accuracy during cross validation for all datasets.

Table 11: Optimal hyperparameters determined and highest accuracy achieved during model cross validation.

dataset	descriptors	number of trees	split criterion	share of attributes per split	Share of samples per tree	mean accuracy	std. dev. of accuracy
LIBS separately measured	(b)	100	gini	0.2	1	0.995	0.006
Tandem dataset	(b)+all Ions	100	gini	0.2	1	0.995	0.006
LIBS separately measured	reduced	150	gini	0.1	0.75	0.994	0.008
Tandem dataset	reduced	100	entropy	0.2	0.75	0.995	0.008

It should be noted that the selection of the split criterion does not seem to have a noticeable effect on the performance of the model, as well as the share of attributes per split, if it is 0.1 or above.

4.3.2 Matthews Correlation Coefficient of cross-validation

Using the hyperparameters obtained in the previous step, a second cross validation was performed, this time keeping track of the results for each sample class separately. From these confusion matrices, the Matthews correlation coefficient (MCC) [75],also called phi coefficient [76], for each molding compound class was calculated using the true positive (TP), true negative (TN), false positive (FP) and false negative (FN) rates for each sample class.

$$MCC = \frac{TP \cdot TN - FP \cdot FN}{\sqrt{(TP + FP) \cdot (TP + FN) \cdot (TN + FP) \cdot (TN + FN)}}$$

The Matthews correlation coefficient ranges from -1 to 1, whereby 0 means no correlation, 1 perfect accordance (only TP and TN) and -1 inverse relation (only FP and FN).

Mean value and standard deviation of the Matthews correlation coefficients for all 10 cross-validation repetitions for each molding compound type are shown in Figure 34. For each type, the mean of the correlation coefficient is well above 0.9 in both datasets for both descriptor sets. The standard deviation of the LIBS dataset is higher than that of the Tandem dataset.

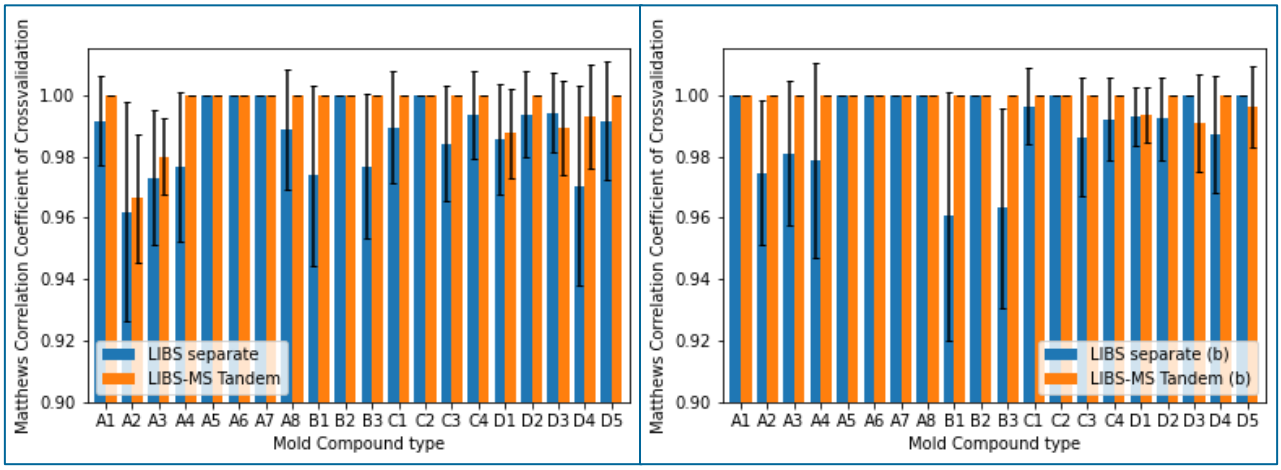

Figure 34: Matthews correlation coefficient during cross-validation for each molding compound type separately. Left: reduced dataset, right: dataset with all elements included

4.3.3 Feature importance

To make out the most influential attributes in the models, the mean decrease in impurity contributed by each attribute was calculated in 10 fold cross-validation, using 70 % of the training set in each fold. The results are shown in Figure 35 and Figure 36 in the form of a box plot. The features are sorted by their mean feature importance in descending order. The box extends from the first to the third quartile with a horizontal line marking the median. The whiskers extend from the box for 1.5 times the interquartile range, datapoints outside this range are depicted as diamonds.

In the case of the LIBS dataset, the feature importance is distributed over a large number of attributes. Features that contribute more than 2 % to the decrease in impurity are emission lines of elements C, H, O, Al, Si, Zn, Mg, Ca, and Sb as well as the C_2 molecule. Emission lines of B, Mo, Zr and Bi only play a minor part.

The distribution of feature importance in the Tandem dataset is more concentrated. Only a few LIBS emission lines of C, H, Al, Si, Zn an Mg contribute more than 2 % to the decrease in impurity. Most of the top spots are taken by MS ion intensities, with only ^{178}Hf falling below the 2 % threshold.

The feature importance of the models using the full descriptor sets closely resembles the reduced data sets results, with only Li and Na surpassing the 2 % threshold.

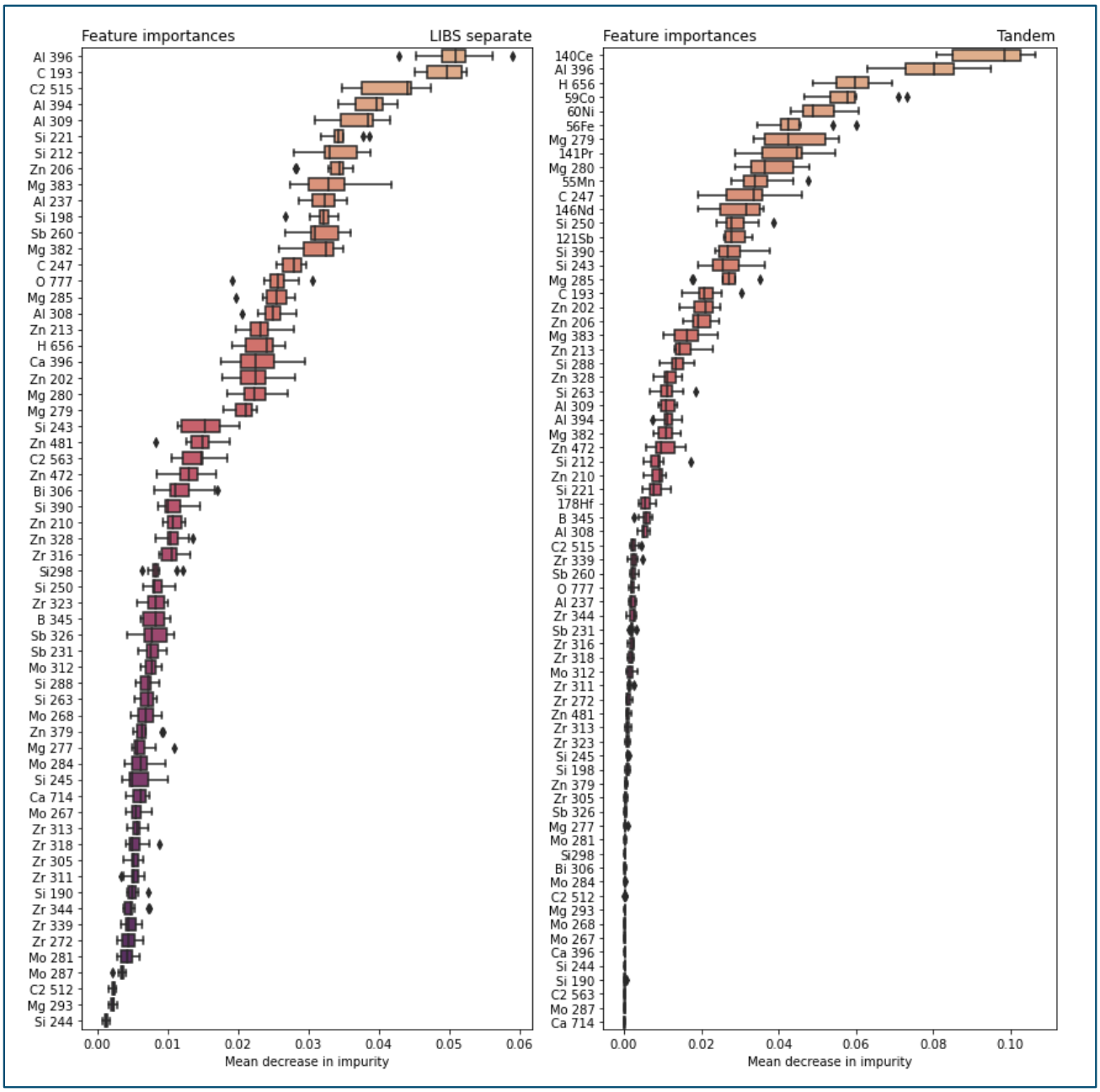

Figure 35: Feature importance for all attributes used for model generation calculated as mean decrease in impurity during cross-validation for the separately measured LIBS dataset (left) and the Tandem dataset (right) with reduced descriptor set.

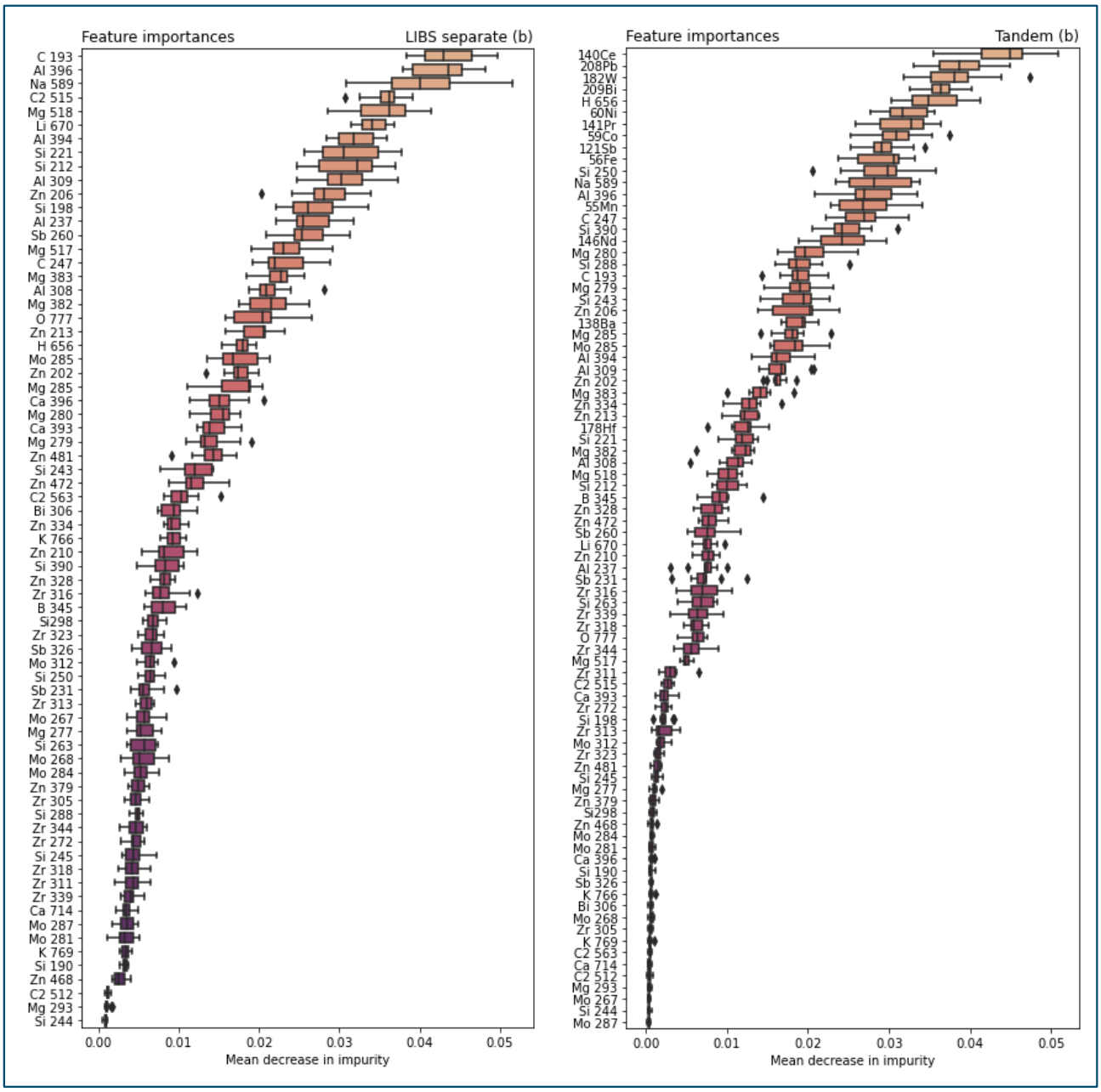

Figure 36: Feature importance for all attributes used for model generation calculated as mean decrease in impurity during cross-validation for the separately measured LIBS dataset (left) and the Tandem dataset (right) with full descriptor set.

4.3.4 Final validation

The cross validation demonstrated that Random decision forest models using the selected hyperparameters are successful at correctly classifying data measured from the same piece of molding compound than the training data. In a real world application, the unknown data seldom originates from the same piece of material as data contained in the training set, as the class of a specific sample is either known or unknown. This situation is simulated by the choice of training and test set. The advantage of this approach is a more meaningful result of the final validation. The disadvantage is that it only allows the validation of the model for molding compound types where at least two different samples were available, resulting in a test set containing only seven different classes. For all other molding compound types, no additional information to the cross validation can be obtained.

For final validation, a classifier with the hyperparameters determined before was trained using all data from the training set and used to classify the data of the test set. The result is presented in Figure 37 and Figure 38 in the form of confusion matrices. The rows represent the true molding compound type (or “class”) of a data point, the columns the class that was predicted by the classifier. Correctly classified data ends up on the diagonal, datapoints off the diagonal were misclassified.

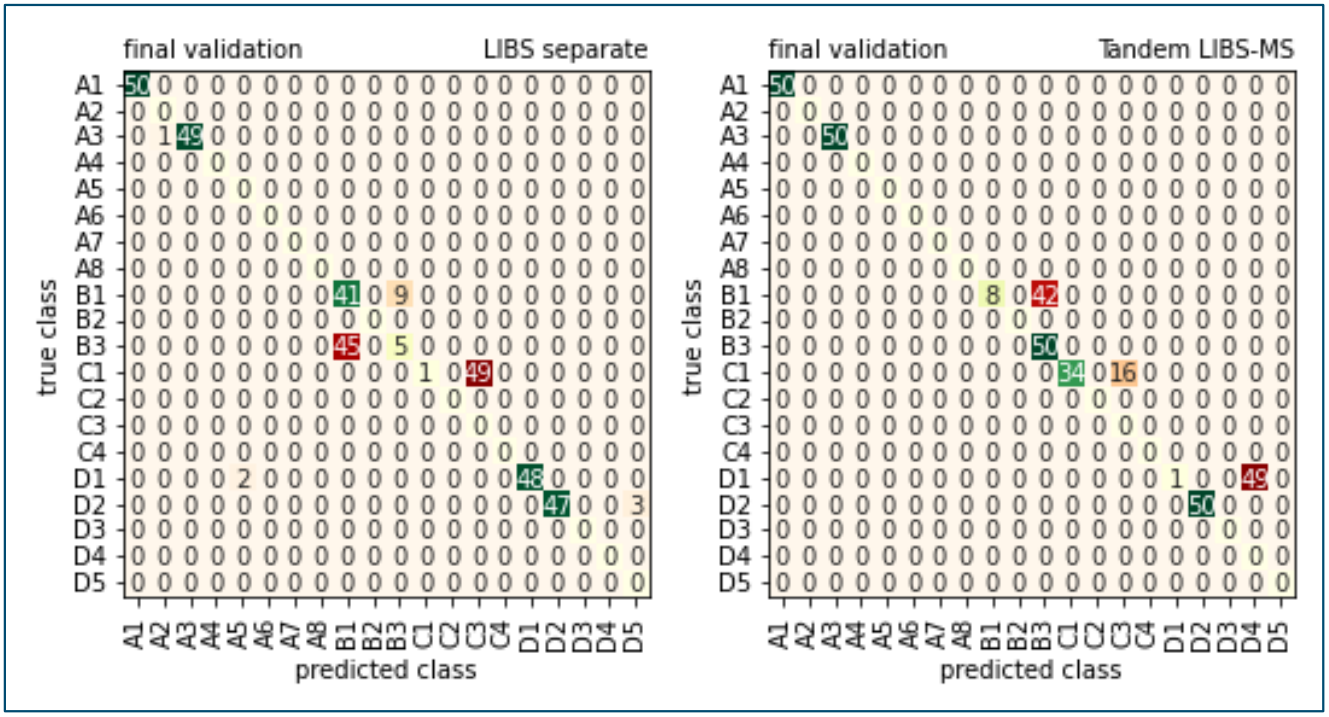

Figure 37: Confusion matrices of the final validation of the Random forest models using the reduced descriptor set.

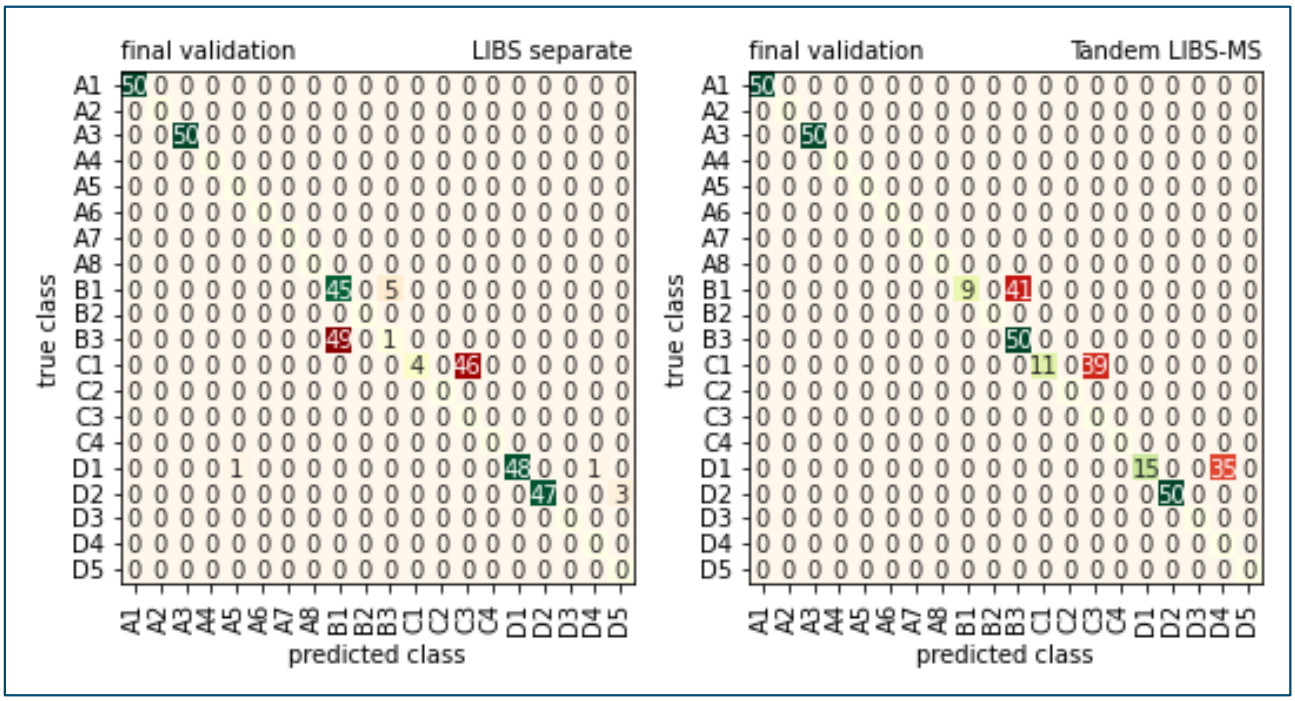

Figure 38: Confusion matrices of the final validation of the Random forest models using the full descriptor set.

The classifiers built on the LIBS dataset achieves a true positive rate of >80 % for five of the seven molding compounds in the test dataset, >90 % for four of them. The classifier built on the tandem dataset achieves a true positive rate of 100 % for four molding compounds.

Problematic are the molding compounds B1 and B3, which can seemingly not be differentiated by the classifiers. Using the LIBS dataset, both are identified as B1, while the Tandem classifier predicts B3 for both. The second error of both classifiers is the misclassification of some or nearly all datapoints of molding compound C1 as class C3. The Tandem classifier additionally misclassified molding compound D1 as D4.

Over all, the models trained on LIBS data alone achieves a slightly better result in classifying the samples of the test data set. This is most likely due to the Tandem models relying heavily on the ion intensities from the ICP-MS for classification, as the feature importance plots have clearly shown. As opposed to the information contained in the LIBS spectra, these are only present in very small amounts in the sample and may well originate from the molding process and tools as opposed to the original molding compound material. For the tandem measurement, some compromise that had to be made in measurement conditions to allow the simultaneous measurement of LIBS and LA-ICP-MS data caused a reduction in the quality of the LIBS spectra. The comparison of the results of the two models suggests that the additional information about trace elements is not worth the trade-off of better quality LIBS spectra and may even hinder the correct classification of new samples, as it attaches undue importance to signals originating from sample contamination.

This final validation experiment confirms the suspicion that some of the molding compound materials are so similar that in some cases the differences between samples introduced in production and handling can outweigh the differences between molding compound types. The inclusion or exclusion of elements like Li, Na and K does not seem to change the performance of the classifier either way, in contrast to the results from the exploratory data analysis. To make the classifier more robust against these influences, more samples of the same type with different origins and sample types would have to be included into the training data. Unfortunately, these were not available for current experiments.

For most molding compounds classification worked really well. The cross validation results also suggest that a training set containing more than 1-2 discrete samples per molding compound type might result in a classifier that is able to correctly identify all 20 molding compound types.

5 Conclusions

The goal of this work, to find ways to characterize and classify epoxy molding compounds to facilitate quality screening and the identification of molding compounds, could be reached for the most part. For this purpose, the samples were examined using various analysis techniques, the data obtained was subsequently used for multivariate analysis. In a first series of preliminary tests, microwave assisted digestions were carried out and the sample solutions produced were analyzed using liquid ICP-MS.

Although total digestion of the sample material was not achieved using a standard approach microwave assisted acid digestion, due to the complexity of the molding compound material, for major inorganic components, such as boron, aluminium and zinc, as well as minor constituents such as cerium, praseodymium and neodymium, significant differences in concentration could be detected in the 10 samples investigated by ICP-MS liquid measurements. For some trace components, such as Sodium and Potassium, the intensities and variations in the background signals (due to insufficient purity of applied reagents and consumables) was too high for confident detection. Quantitative data should be obtainable by further optimisation of the digestion procedure, but was not necessary for this work.

Subsequently, the solid samples were examined using LIBS and LA-ICP-MS, whereby the problems observed during the digestion of the samples - incompleteness, contamination, and high expenditure of time - could be avoided. The results of the ICP-MS measurements proved useful for the selection of elements to investigate in LA-ICP-MS and Tandem LIBS/LA-ICP-MS experiments, as well as providing qualitative information about the molding compound composition.

LIBS measurement results supported the findings of the liquid ICP-MS measurements concerning the content of major inorganic components such as aluminium and magnesium. Furthermore, elements such as carbon, oxygen, hydrogen that were not accessible to ICP-MS analysis could be recorded. In some cases, significant differences in composition were found between the individual samples, for example some samples contained boron and others contained manganese or zirconium. The data obtained was well suited for multivariate data analysis using PCA and HCA. Clustering techniques demonstrated that in some cases the elemental composition is significantly influenced by the sample type (cull, tile, package) as well as the molding compound type.

The additionally conducted LA-ICP-MS measurements only allowed for the analysis of a limited number of elements at a time in contrast to the ICP-MS analysis of the digested liquid samples. Since information about major components is accessible using LIBS, minor components and trace constituents were chosen for LA-ICP-MS analysis. Subsequently, a tandem measurement combining LIBS and LA-ICP-MS measurements was also carried out.

Data sets generated by LIBS, LA-ICP-MS and Tandem measurements were investigated using principal component analysis and hierarchical cluster analysis. A spectral descriptor approach was used for the LIBS data to reduce the dimensionality of the dataset and to facilitate the interpretation of results. A split between measurements of samples of the same molding compound but different sample types (cull, tile, package) was observed in PCA plots. To remove this unwanted separation, reduced descriptor sets without the emission lines of Li, Na and K as well as the ion intensity information of Ba, W, Pb and Bi were tested for random decision forest classification alongside a descriptor set containing this information. The resulting four data sets (LIBS and Tandem data, each with a comprehensive and a reduced set of descriptors) were used for development of a random decision forest classifier.

The data selected for random forest classification was split into independent training and test subsets by selecting whole physical samples as test subset and removing all data points of these samples from the training data. The training subset was used for model optimisation. A 10-fold cross validation was performed for hyperparameter optimisation. All four investigated data sets performed comparably, resulting in mean accuracies during cross validation of above 99 %.

For the training of a random forest classifier, the LIBS data set from the separate measurement seems to perform slightly better than the tandem data set. A classifier built on the LIBS data set using the full descriptor set achieves a true positive rate of >80 % for five of the seven molding compounds in the test dataset. The classifier built on the

tandem dataset achieves a true positive rate of 100 % for four molding compounds, misclassifying one sample that was correctly identified by the classifier built on the LIBS data set.

Possible explanations for this result are the compromise measurement conditions during Tandem measurement that result in lower quality LIBS data, as well as the inclusion of potentially misleading information on trace elements that originate from contamination by the ICP-MS data. The removal of possible contaminant information from the data set (Li, Na and K emission lines and Ba, W, Pb and Bi ion intensities) did not improve the classification results.

LA-ICP-MS and Tandem measurements proved useful for the collection of information of trace element content. Although the inclusion of trace element information did not improve the performance of the random forest classifier, knowledge about possible contamination of the packaging material is potentially useful to ascertain the consistent composition of the material for quality assurance purposes.

The fact that the tandem data set seems to be more sensitive to contamination makes this technique more interesting for quality assurance purposes. If the Tandem measurement of a sample is not correctly classified, this might point to impurities in the material that differ from the training data. The good results of cross validation of all classifiers investigated suggest that random forest classifiers are suitable for the classification of epoxy molding compounds.

To improve on these results in the future, two approaches seem promising: To obtain a more stable classifier and achieve more reliable results in classification of unknown samples, a larger set of physical samples would be beneficial due to the differences between samples of the same mold compound type that were observed. The inclusion of additional measurement techniques that deliver more polymer specific information, such as Pyrolysis-GC-MS[77] analysis, might prove beneficial as well.

6 Bibliography

[1] 'Semiconductor Market Size & Share | Industry Growth [2029]'. https://www.fortunebusinessinsights.com/semiconductor-market-102365 (accessed Jun. 15, 2022).

[2] L. Lay Yeap, 'Meeting the assembly challenges in new semiconductor packaging trend', in *2010 34th IEEE/CPMT International Electronic Manufacturing Technology Symposium (IEMT)*, Nov. 2010, pp. 1–5. doi: 10.1109/IEMT.2010.5746731.

[3] B. Fuchs, S. Vogel, and D. Schroeder, 'Universal application-specific integrated circuit for bioelectric data acquisition', *Medical Engineering & Physics*, vol. 24, no. 10, pp. 695–701, Dec. 2002, doi: 10.1016/S1350-4533(02)00117-0.

[4] H. Zheng, G. Shi, T. Zeng, and B. Li, 'Wireless earthquake alarm design based on MEMS accelerometer', in *2011 International Conference on Consumer Electronics, Communications and Networks (CECNet)*, Apr. 2011, pp. 5481–5484. doi: 10.1109/CECNET.2011.5768502.

[5] A. T. So and W. L. Chan, 'Fire Protection Systems', in *Intelligent Building Systems*, A. T. So and W. L. Chan, Eds. Boston, MA: Springer US, 1999, pp. 35–38. doi: 10.1007/978-1-4615-5019-8_5.

[6] William J. Greig, *Integrated Circuit Packaging, Assembly and Interconnections*. Boston, MA: Springer US, 2007. doi: 10.1007/0-387-33913-2.

[7] W. Lambrechts and S. Sinha, 'A Review on Si, SiGe, GaN, SiC, InP and GaAs as Enabling Technologies in EW and Space', in *SiGe-based Re-engineering of Electronic Warfare Subsystems*, W. Lambrechts and S. Sinha, Eds. Cham: Springer International Publishing, 2017, pp. 301–329. doi: 10.1007/978-3-319-47403-8_10.

[8] 'Wire Bonding Guidelines | AmTECH Microelectronics'. https://amtechmicro.com/guidelines/wire-bonding-guidelines/ (accessed Jul. 22, 2022).

[9] O. Brand, '1.15 - Packaging', in *Comprehensive Microsystems*, Y. B. Gianchandani, O. Tabata, and H. Zappe, Eds. Oxford: Elsevier, 2008, pp. 431–463. doi: 10.1016/B978-044452190-3.00019-7.

[10] N. Kinjo, M. Ogata, K. Nishi, A. Kaneda, and K. Dušek, 'Epoxy Molding Compounds as Encapsulation Materials for Microelectronic Devices', in *Speciality Polymers/Polymer Physics*, Berlin, Heidelberg, 1989, pp. 1–48. doi: 10.1007/BFb0017963.

[11] 'Integrated Circuit Package Types And Thermal Characteristics', *Electronics Cooling*, Feb. 09, 2006. https://www.electronics-cooling.com/2006/02/integrated-circuit-package-types-and-thermal-characteristics/ (accessed Jul. 22, 2022).

[12] R. Plieninger, M. Dittes, and K. Pressel, 'Modern IC packaging trends and their reliability implications', *Microelectronics Reliability*, vol. 46, no. 9, pp. 1868–1873, Sep. 2006, doi: 10.1016/j.microrel.2006.08.008.

[13] L. Xiao-ling, L. Jian-wen, and Z. Liang-biao, 'Influence of package failure on IC's reliability', in *2013 14th International Conference on Electronic Packaging Technology*, Aug. 2013, pp. 114–117. doi: 10.1109/ICEPT.2013.6756435.

[14] M. A. Bahi, P. Lecuyer, H. Fremont, and J.-P. Landesman, 'Sequential environmental stresses tests qualification for automotive components', *Microelectronics Reliability*, vol. 47, no. 9, pp. 1680–1684, Sep. 2007, doi: 10.1016/j.microrel.2007.07.004.

[15] A. Inamdar *et al.*, 'Study of thermal aging behavior of epoxy molding compound for applications in harsh environments: 69th IEEE Electronic Components and Technology Conference, ECTC 2019', *Proceedings - IEEE 69th Electronic Components and Technology Conference, ECTC 2019*, pp. 811–818, May 2019, doi: 10.1109/ECTC.2019.00128.

[16] A. Inamdar, Y.-H. Yang, A. Prisacaru, P. Gromala, and B. Han, 'High temperature aging of epoxy-based molding compound and its effect on mechanical behavior of molded electronic package', *Polymer Degradation and Stability*, vol. 188, p. 109572, Jun. 2021, doi: 10.1016/j.polymdegradstab.2021.109572.

[17] R. Li, D. Yang, P. Zhang, F. Niu, M. Cai, and G. Zhang, 'Effects of High-Temperature Storage on the Elasticity Modulus of an Epoxy Molding Compound', *Materials (Basel)*, vol. 12, no. 4, p. 684, Feb. 2019, doi: 10.3390/ma12040684.

[18] I. Fukuzawa, S. Ishiguro, and S. Nanbu, 'Moisture Resistance Degradation of Plastic LSIs by Reflow Soldering', in *23rd International Reliability Physics Symposium*, Mar. 1985, pp. 192–197. doi: 10.1109/IRPS.1985.362097.

[19] *Moisture Sensitivity of Plastic Packages of IC Devices*. Accessed: Jul. 20, 2022. [Online]. Available: https://link.springer.com/book/10.1007/978-1-4419-5719-1

[20] M. Zhang, S. W. R. Lee, J. Zhang, H. Yun, D. Starkey, and H. Chau, 'Correlation between material selection and moisture sensitivity levels of quad flat no-lead (QFN) packages', in *2009 European Microelectronics and Packaging Conference*, Jun. 2009, pp. 1–6.

[21] M. van Soestbergen, R. T. H. Rongen, L. J. Ernst, and G. Q. Zhang, 'Modeling ion transport through molding compounds and its relation to product reliability', in *2008 International Conference on Electronic Packaging Technology & High Density Packaging*, Jul. 2008, pp. 1–8. doi: 10.1109/ICEPT.2008.4606987.

[22] S. Schwab, J. Jung, S. Gruber, M. Bauer, M. Nelhiebel, and H. Hutter, 'Characterization of Electric Field Induced Ion Migration in Semiconductor Encapsulation Materials', *Meet. Abstr.*, vol. MA2015-02, no. 24, p. 955, Jul. 2015, doi: 10.1149/MA2015-02/24/955.

[23] L. Lantz and M. G. Pecht, 'Ion transport in encapsulants used in microcircuit packaging', *IEEE Transactions on Components and Packaging Technologies*, vol. 26, no. 1, pp. 199–205, Mar. 2003, doi: 10.1109/TCAPT.2002.806183.

[24] F. Bohrn *et al.*, 'Study on the Ion Migration of Silver Ions from Aqueous Solution in Epoxy-Based Molding Compounds by TOF-SIMS Measurements', *ECS J. Solid State Sci. Technol.*, vol. 11, no. 2, p. 024006, Feb. 2022, doi: 10.1149/2162-8777/ac546b.

[25] K. Holland-moritz and H. W. Siesler, 'Infrared Spectroscopy of Polymers', *Applied Spectroscopy Reviews*, vol. 11, no. 1, pp. 1–55, Jan. 1976, doi: 10.1080/05704927608081704.

[26] R. Leitner, H. Mairer, and A. Kercek, 'Real-time classification of polymers with NIR spectral imaging and blob analysis', *Real-Time Imaging*, vol. 9, no. 4, pp. 245–251, Aug. 2003, doi: 10.1016/j.rti.2003.09.016.

[27] T. Zhang, D. Xia, H. Tang, X. Yang, and H. Li, 'Classification of steel samples by laser-induced breakdown spectroscopy and random forest', *Chemometrics and Intelligent Laboratory Systems*, vol. 157, pp. 196–201, Oct. 2016, doi: 10.1016/j.chemolab.2016.07.001.

[28] L. Sheng *et al.*, 'Classification of iron ores by laser-induced breakdown spectroscopy (LIBS) combined with random forest (RF)', *Journal of Analytical Atomic Spectrometry*, vol. 30, no. 2, pp. 453–458, 2015, doi: 10.1039/C4JA00352G.

[29] J. Qi, T. Zhang, H. Tang, and H. Li, 'Rapid classification of archaeological ceramics via laser-induced breakdown spectroscopy coupled with random forest', *Spectrochimica Acta Part B: Atomic Spectroscopy*, vol. 149, pp. 288–293, Nov. 2018, doi: 10.1016/j.sab.2018.09.006.

[30] 'Semiconductor - Epoxy Molding Compund (EMC) | Samsung SDI'. https://www.samsungsdi.com/electronic-materials/semiconductor/emc-epoxy-molding-compound.html (accessed Feb. 03, 2022).

[31] A. Hayakawa, Y. Murata, Y. Nakanishi, and N. Tohriiwa, 'Epoxy resin composition for semiconductor encapsulation', US5739186A, Apr. 14, 1998 Accessed: Feb. 28, 2022. [Online]. Available: https://patents.google.com/patent/US5739186A/en

[32] 'Polymers in Electronic Packaging Part One: Introduction to Mold Compounds', *Polymer Innovation Blog*, Mar. 27, 2017. https://polymerinnovationblog.com/polymers-electronic-packaging-part-one-introduction-mold-compounds/ (accessed Feb. 28, 2022).

[33] 'sample digestion'. https://www.ebi.ac.uk/ols/ontologies/chmo/terms?iri=http%3A%2F%2Fpurl.obolibrary.org%2Fobo%2FCHMO_0001489 (accessed Jun. 07, 2022).

[34] Adel. Abu-Samra, J. Steven. Morris, and S. R. Koirtyohann, 'Wet ashing of some biological samples in a microwave oven', *Anal. Chem.*, vol. 47, no. 8, pp. 1475–1477, Jul. 1975, doi: 10.1021/ac60358a013.

[35] 'Microwave Reaction System for Sample Preparation: Multiwave PRO'. http://www.sisc.com.vn/en/detail.php?module=product&iCat=1463&iData=684&#page=page-3 (accessed Mar. 04, 2022).

[36] D. L. Rocha, A. D. Batista, F. R. P. Rocha, G. L. Donati, and J. A. Nóbrega, 'Greening sample preparation in inorganic analysis', *TrAC Trends in Analytical Chemistry*, vol. 45, pp. 79–92, Apr. 2013, doi: 10.1016/j.trac.2012.12.015.

[37] 'Mikrowellenaufschluss-Plattform: Multiwave 5000 :: Anton-Paar.com', *Anton Paar*. https://www.anton-paar.com/at-de/produkte/details/multiwave-5000/ (accessed May 27, 2022).

[38] J. S. Becker, *Inorganic Mass Spectrometry: Principles and Applications*. John Wiley & Sons Ltd, 2007.

[39] 'What is Single Particle ICP-MS?', *TOFWERK*, Jan. 04, 2018. https://www.tofwerk.com/single-particle-icp-ms/ (accessed Jun. 07, 2022).

[40] C. J. Barinaga, D. W. Koppenaal, and S. A. McLuckey, 'Ion-trap mass spectrometry with an inductively coupled plasma source', *Rapid Communications in Mass Spectrometry*, vol. 8, no. 1, pp. 71–76, 1994, doi: 10.1002/rcm.1290080114.

[41] K. E. Milgram *et al.*, 'High-Resolution Inductively Coupled Plasma Fourier Transform Ion Cyclotron Resonance Mass Spectrometry', *Anal. Chem.*, vol. 69, no. 18, pp. 3714–3721, Sep. 1997, doi: 10.1021/ac970126n.

[42] W. Henderson and J. S. McIndoe, 'Mass Analysers', in *Mass Spectrometry of Inorganic, Coordination and Organometallic Compounds*, John Wiley & Sons, Ltd, 2005, pp. 23–46. doi: 10.1002/0470014318.ch2.

[43] W. Paul and H. Steinwedel, 'Apparatus for separating charged particles of different specific charges', US2939952A, Jun. 07, 1960 Accessed: Apr. 06, 2022. [Online]. Available: https://patents.google.com/patent/US2939952A/en

[44] D. W. Koppenaal, G. C. Eiden, and C. J. Barinaga, 'Collision and reaction cells in atomic mass spectrometry: development, status, and applications', *J. Anal. At. Spectrom.*, vol. 19, no. 5, pp. 561–570, May 2004, doi: 10.1039/B403510K.

[45] M. E. Wieser and J. B. Schwieters, 'The development of multiple collector mass spectrometry for isotope ratio measurements', *International Journal of Mass Spectrometry*, vol. 242, no. 2, pp. 97–115, Apr. 2005, doi: 10.1016/j.ijms.2004.11.029.

[46] I. Rodushkin and M. D. Axelsson, 'Application of double focusing sector field ICP-MS for multielemental characterization of human hair and nails. Part I. Analytical methodology', *Science of The Total Environment*, vol. 250, no. 1, pp. 83–100, Apr. 2000, doi: 10.1016/S0048-9697(00)00369-7.

[47] S. Takac and S. Stojanović, '[Characteristics of laser light]', *Med Pregl*, vol. 52, no. 1–2, pp. 29–34, Jan. 1999.

[48] David A.Cremers, Leon J. Radziemski, *Handbook of Laser-Induced Breakdown Spectroscopy*, 2nd ed. John Wiley and Sons, Ltd.

[49] Donald C. O'Shea, *Introduction to Lasers and Their Applications*. Addison-Wesley Publishing Company.

[50] DIN German Institute for Standardization, 'Surface chemical analysis – Vocabulary – Part 1: General terms and terms used in spectroscopy (ISO 18115-1:2016-9)'. Accessed: May 20, 2022. [Online]. Available: https://www.en-standard.eu/din-iso-18115-1-surface-chemical-analysis-vocabulary-part-1-general-terms-and-terms-used-in-spectroscopy-iso-18115-1-2013/

[51] G. Hughes, 'On the mean accuracy of statistical pattern recognizers', *IEEE Transactions on Information Theory*, vol. 14, no. 1, pp. 55–63, Jan. 1968, doi: 10.1109/TIT.1968.1054102.

[52] H. Lohninger and J. Ofner, 'Multisensor hyperspectral imaging as a versatile tool for image-based chemical structure determination', *Spectrosc. Eur*, vol. 26, no. 5, pp. 6–10, 2014.

[53] V. N. G. Raju, K. P. Lakshmi, V. M. Jain, A. Kalidindi, and V. Padma, 'Study the Influence of Normalization/Transformation process on the Accuracy of Supervised Classification', in *2020 Third International Conference on Smart Systems and Inventive Technology (ICSSIT)*, Aug. 2020, pp. 729–735. doi: 10.1109/ICSSIT48917.2020.9214160.

[54] O. Maimon and L. Rokach, *Data Mining and Knowledge Discovery Handbook*. Springer Science & Business Media, 2006.

[55] C. Cheng, 'Principal Component Analysis (PCA) Explained Visually with Zero Math', *Medium*, Mar. 22, 2022. https://towardsdatascience.com/principal-component-analysis-pca-explained-visually-with-zero-math-1cbf392b9e7d (accessed Aug. 22, 2022).

[56] Leonard Kaufman and Peter J. Rousseeuw, 'Introduction', in *Finding Groups in Data*, John Wiley & Sons, Ltd, 1990, pp. 1–67. doi: 10.1002/9780470316801.ch1.

[57] J. H. Ward, 'Hierarchical Grouping to Optimize an Objective Function', *Journal of the American Statistical Association*, vol. 58, no. 301, pp. 236–244, Mar. 1963, doi: 10.1080/01621459.1963.10500845.

[58] '3.1. Cross-validation: evaluating estimator performance', *scikit-learn*. https://scikit-learn/stable/modules/cross_validation.html (accessed Jun. 07, 2022).

[59] L. Breiman, 'Technical Note: Some Properties of Splitting Criteria', *Machine Learning*, vol. 24, no. 1, pp. 41–47, Jul. 1996, doi: 10.1023/A:1018094028462.

[60] T. Jo, *Machine Learning Foundations: Supervised, Unsupervised, and Advanced Learning*. Cham: Springer International Publishing, 2021. doi: 10.1007/978-3-030-65900-4.

[61] L. Breiman, 'Random Forests', *Machine Learning*, vol. 45, no. 1, pp. 5–32, Oct. 2001, doi: 10.1023/A:1010933404324.

[62] '1.11. Ensemble methods', *scikit-learn*. https://scikit-learn/stable/modules/ensemble.html (accessed Jun. 09, 2022).

[63] Asoke Nandi and Hosameldin Ahmed, 'Decision Trees and Random Forests', in *Condition Monitoring with Vibration Signals*, John Wiley & Sons, Ltd, 2019, pp. 199–224. doi: 10.1002/9781119544678.ch10.

[64] W. McKinney, 'Data Structures for Statistical Computing in Python', Austin, Texas, 2010, pp. 56–61. doi: 10.25080/Majora-92bf1922-00a.

[65] F. Pedregosa *et al.*, 'Scikit-learn: Machine Learning in Python', *Journal of Machine Learning Research*, vol. 12, no. 85, pp. 2825–2830, 2011, Accessed: Jun. 07, 2022. [Online]. Available: http://jmlr.org/papers/v12/pedregosa11a.html

[66] J. D. Hunter, 'Matplotlib: A 2D Graphics Environment', *Computing in Science & Engineering*, vol. 9, no. 3, pp. 90–95, May 2007, doi: 10.1109/MCSE.2007.55.

[67] I. Flyamer *et al.*, 'Phlya/adjustText: 0.8 beta'. Zenodo, Jun. 30, 2020. doi: 10.5281/zenodo.3924114.

[68] M. Dogan, S. D. Dogan, L. A. Savas, G. Ozcelik, and U. Tayfun, 'Flame retardant effect of boron compounds in polymeric materials', *Composites Part B: Engineering*, vol. 222, p. 109088, Oct. 2021, doi: 10.1016/j.compositesb.2021.109088.

[69] R. Höfer, '10.21 - Processing and Performance Additives for Plastics', in *Polymer Science: A Comprehensive Reference*, K. Matyjaszewski and M. Möller, Eds. Amsterdam: Elsevier, 2012, pp. 369–381. doi: 10.1016/B978-0-444-53349-4.00272-7.

[70] R. N. Rothon and P. R. Hornsby, 'Flame retardant effects of magnesium hydroxide', *Polymer Degradation and Stability*, vol. 54, no. 2, pp. 383–385, Nov. 1996, doi: 10.1016/S0141-3910(96)00067-5.

[71] Z. Xu, H. Jia, L. Yan, Z. Chu, and H. Zhou, 'Synergistic effect of bismuth oxide and mono-component intumescent flame retardant on the flammability and smoke suppression properties of epoxy resins', *Polymers for Advanced Technologies*, vol. 31, no. 1, pp. 25–35, 2020, doi: 10.1002/pat.4744.

[72] A. H. Uddin, R. S. Khalid, M. Alaama, A. M. Abdualkader, A. Kasmuri, and S. A. Abbas, 'Comparative study of three digestion methods for elemental analysis in traditional medicine products using atomic absorption spectrometry', *Journal of Analytical Science and Technology*, vol. 7, no. 1, p. 6, Jan. 2016, doi: 10.1186/s40543-016-0085-6.

[73] I. W. Croudace, 'A possible error source in silicate wet-chemistry caused by insoluble fluorides', *Chemical Geology*, vol. 31, pp. 153–155, Jan. 1980, doi: 10.1016/0009-2541(80)90074-1.

[74] J. El Haddad, L. Canioni, and B. Bousquet, 'Good practices in LIBS analysis: Review and advices', *Spectrochimica Acta Part B: Atomic Spectroscopy*, vol. 101, pp. 171–182, Nov. 2014, doi: 10.1016/j.sab.2014.08.039.

[75] B. W. Matthews, 'Comparison of the predicted and observed secondary structure of T4 phage lysozyme', *Biochimica et Biophysica Acta (BBA) - Protein Structure*, vol. 405, no. 2, pp. 442–451, Oct. 1975, doi: 10.1016/0005-2795(75)90109-9.

[76] G. U. Yule, 'On the Methods of Measuring Association Between Two Attributes', May 1912, doi: 10.2307/2340126.

[77] R. Rial-Otero, M. Galesio, J.-L. Capelo, and J. Simal-Gándara, 'A Review of Synthetic Polymer Characterization by Pyrolysis–GC–MS', *Chroma*, vol. 70, no. 3, pp. 339–348, Aug. 2009, doi: 10.1365/s10337-009-1254-1.

7 List of figures

8 List of tables